Contrib Mineral Petrol (2008) 155:271–293
DOI 10.1007/s00410-007-0241-5

ORIGINAL PAPER

Evolution of subcontinental lithospheric mantle beneath eastern China: Re–Os isotopic evidence from mantle xenoliths in Paleozoic kimberlites and Mesozoic basalts

Hong-Fu Zhang · Steven L. Goldstein · Xin-Hua Zhou · Min Sun · Jian-Ping Zheng · Yue Cai

Received: 30 January 2007 / Accepted: 12 July 2007 / Published online: 3 August 2007

Abstract The ages of subcontinental lithospheric mantle beneath the North China and South China cratons are less well-constrained than the overlying crust. We report Re–Os isotope systematics of mantle xenoliths entrained in Paleozoic kimberlites and Mesozoic basalts from eastern China. Peridotite xenoliths from the Fuxian and Mengyin Paleozoic diamondiferous kimberlites in the North China Craton give Archean Re depletion ages of 2.6–3.2 Ga and melt depletion ages of 2.9–3.4 Ga. No obvious differences in Re and Os abundances, Os isotopic ratios and model ages are observed between spinel-facies and garnet-facies peridotites from both kimberlite localities. The Re–Os isotopic data, together with the PGE concentrations, demonstrate that beneath the Archean continental crust of the eastern North China Craton, Archean lithospheric mantle of spinel- to diamond-facies existed without apparent compositional stratification during the Paleozoic. The Mesozoic and Cenozoic basalt-borne peridotite and pyroxenite xenoliths, on the other hand, show geochemical features indicating metasomatic enrichment, along with a large range of the Re–Os isotopic model ages from Proterozoic to Phanerozoic. These features indicate that lithospheric transformation or refertilization through melt-peridotite interaction could be the primary mechanism for compositional changes during the Phanerozoic, rather than delamination or thermal-mechanical erosion, despite the potential of these latter processes to play an important role for the loss of garnet-facies mantle. A fresh garnet lherzolite xenolith from the Yangtze Block has a Re depletion age of $\sim$1.04 Ga, much younger than overlying Archean crustal rocks but the same Re depletion ages as spinel lherzolite xenoliths from adjacent Mesozoic basalts, indicating Neoproterozoic resetting of the Re–Os system in the South China Craton.

Keywords Eastern China · Mantle xenoliths · Re–Os isotopes · PGEs · Subcontinental lithospheric mantle · Re depletion ages

Communicated by T. L. Groove.

H.-F. Zhang (✉) · X.-H. Zhou
State Key Laboratory of Lithospheric Evolution,
Institute of Geology and Geophysics,
Chinese Academy of Sciences,
P.O. Box 9825, Beijing 100029, China
e-mail: hfzhang@mail.igcas.ac.cn

S. L. Goldstein (✉) · Y. Cai
Lamont-Doherty Earth Observatory and Department of Earth and Environmental Sciences, Columbia University, 61 Rt. 9W, Palisades, NY 10964, USA
e-mail: steveg@ldeo.columbia.edu

M. Sun
Department of Earth Sciences, The University of Hong Kong, Pokfulam Road, Hong Kong, China

J.-P. Zheng
State Key Laboratory of Geological Processes and Mineral Resources, China University of Geosciences, Wuhan 430074, China

Introduction

While the details of the mechanism of Archean continental crust formation are still a matter of debate, it is clear that it involves partial melting of the upper mantle, resulting in depletion of FeO, CaO, Al_2O_3 and alkalis, and enrichment of MgO in the melt residue, which becomes the subcontinental lithospheric mantle (SCLM) (e.g., Jordan 1975, 1988; Boyd et al. 1985; Pollack 1986; Rudnick and Fountain 1995; King 2005). As a consequence of this

depletion process, the residual SCLM has a lower density (about 3.0 g/cm^3) than the asthenosphere (about 3.35 g/cm^3), which helps to stabilize ancient cratonic lithosphere and explains why it behaves as a rigid plate in the scheme of global plate tectonics. This further implies that the structure of Archean cratons is such that Archean continental crust is underlain by Archean age lithospheric mantle, composed of highly refractory spinel-, garnet- to diamond-facies peridotite. This model for the structure of Archean cratons appears to be valid in southern Africa, as evidenced by mineral, geochemical and Re–Os isotopic studies on mantle peridotitic xenoliths from kimberlites of the Kaapvaal Craton (Richardson et al. 1984, 1985; Pearson et al. 1995; Pearson 1999).

While the lithospheric mantle beneath the Kaapvaal and Siberian cratons has been stable since their formation (Boyd 1989; Boyd et al. 1985, 1997; Pearson et al. 1995; King 2005), this is not the case for the North China Craton (Fig. 1). Here the thick and cold cratonic lithospheric mantle remained intact through the Paleozoic, but had become a thinner and hotter lithospheric mantle with oceanic affinity by the Cenozoic, as shown by data from mantle xenoliths entrained in the Paleozoic kimberlites and Cenozoic basalts (e.g., Fan and Menzies 1992; Griffin et al. 1992, 1998; Menzies et al. 1993; Menzies and Xu 1998; Zheng and Lu 1999; Fan et al. 2000; Xu 2001; Zheng et al. 2001; Rudnick et al. 2004). This means that a dramatic physico-chemical change occurred during the intervening time interval (e.g., Xu et al. 1998; Zheng et al. 1998; O'Reilly et al. 2001; Gao et al. 2002; Zhang et al. 2002, 2003, 2004; Wilde et al. 2003; Wu et al. 2003; Deng et al. 2004; Zhang 2005; Ying et al. 2006). The North China Cration thus offers an excellent opportunity to address the cause and mechanism of the lithospheric thinning, and the process for the compositional transformation or refertilization of the lithospheric mantle.

Mechanisms invoked for lithospheric thinning in eastern Asia include (1) delamination (Wu et al. 2003; Gao et al. 2004), (2) extension due to a mantle plume (Deng et al. 1994, 2004), and (3) collision between the Indian and Eurasian Plates along with subduction of the Paleo-Pacific Plate (Menzies et al. 1993). However, these explanations are not widely accepted, because (1) eclogite xenoliths are rare in the Paleozoic kimberlites and Mesozoic basalts; (2) Mesozoic plume-related magmatism has not been identified on the North China Craton; and (3) the collision between the Indian and Eurasian Plates occurred later than the Mesozoic (at ~45 Ma). Based on the co-existence of high-Mg# and low-Mg# mantle xenoliths in the Cenozoic basalts from the Hebi region (Fig. 1) in Henan Province, Zheng et al. (2001) suggested that old refractory lithospheric mantle was replaced by young fertile compositions. Menzies and Xu (1998) and Xu (2001) noted the close relationship between the timing of lithospheric thinning and the collision of the North China Craton and the Yangtze Block. They argued that the collision changed the stress-state and stability of the lithospheric mantle, leading to thermal and mechanical erosion at the base of the lithosphere by the upwelling of hot asthenosphere. The widespread occurrence of isotopically enriched mafic rocks and carbonatites of Mesozoic age on the southeastern North China Craton (Fig. 1) demonstrate that subducted materials of the Yangtze lithosphere greatly contributed to generating enriched lithospheric mantle in this region during this time (Qiu et al. 2002; Zhang et al. 2002; Zhang and Sun 2002; Ying et al. 2004; Xu et al. 2004; Fan et al. 2004; Wang et al. 2005). The subduction also triggered alkaline magmatism, as reflected by syenites and

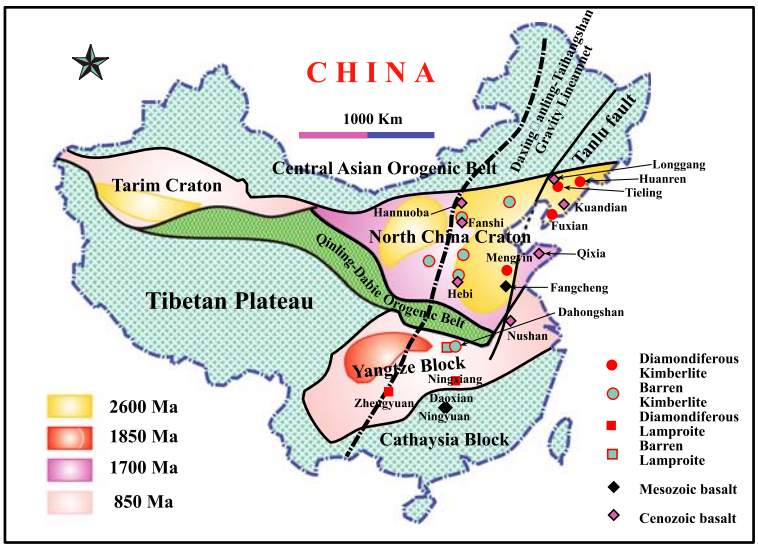

Fig. 1 Simplified tectonic units of China and localities of diamondiferous and barren kimberlite fields (modified from Zhang et al. 1994). The North China Craton consists of two Archean nuclei, the Jiluliao nucleus in the east (the Eastern Block, Zhao et al. (2000)) and the Ordos nucleus in the west (the Western Block). The *solid dash line* extending roughly north-south direction shows the Daxing'anling-Taihangshan Gravity Lineamnet. Also shown are the Paleozoic kimberlite fields, Mesozoic basalts and Cenozoic basalts in eastern China mentioned in the text

monzonites occurring in a belt along the southern portion of the North China Craton (Zhang et al. 2005), generally parallel to the Qinling-Dabie orogenic belt. These observations led to the suggestion that subduction of the Yangtze lithosphere and subsequent collision with the North China Craton may have been the driving force for the rapid transformation of old refractory lithospheric mantle to fertile lithospheric mantle through melt-peridotite interaction during the Mesozoic, especially in the southern portion of the North China Craton (Zhang et al. 2002, 2007; Zhang and Sun 2002, Fan et al. 2004; Wang et al. 2005; Zhang 2005; Zheng et al. 2006a, b). However, these interpretations have not been widely accepted, and the key issue of the mechanism and dynamics of lithospheric thinning still remains controversial.

If the lithospheric mantle had an Archean age prior to the thinning, the Re–Os model ages (c.f. Shirey and Walker 1998) of the present-day lithospheric mantle can rigorously test the abovementioned models for lithospheric thinning. Delamination implies that the present-day lithospheric mantle should have young Re–Os model ages, since it has been newly accreted since the Paleozoic. If the thermo-mechanical erosion model is correct, the remaining lithospheric mantle should have Archean ages. As a third alternative, the compositional transformation model implies coexistence of both old and young ages. Until now, reliable Re–Os model age data for mantle peridotites of the North China Craton are rare, especially for peridotitic xenoliths from Paleozoic kimberlites (Gao et al. 2002; Wu et al. 2003, 2006). Pioneering work on two peridotitic xenoliths from the Fuxian diamondiferous kimberlites (Gao et al. 2002) indicates that the Archean lithospheric mantle existed beneath this region (Fig. 1) of the North China Craton. However, in the Mengyin kimberlites of the central Eastern Block of the North China Craton (Fig. 1) a peridotitic xenolith gives a much younger Mesoproterozoic "Re depletion age" (T_{RD} determined by the time that the present-day $^{187}Os/^{188}Os$ of a sample matched the primitive mantle; c.f. Shirey and Walker 1998) of ~1.46 Ga (Gao et al. 2002), while a chromite separate yielded an Archean T_{RD} of 2.69 Ga (Wu et al. 2006). However, the complex origin of the chromite separate raises question about the implication of this "age". Analyses of chromite separates from Fuxian and Tieling kimberlites (Fig. 1) give much younger Paleoproterozoic T_{RD} of 1.56–1.77 Ga, at the same time giving old Paleoproterozoic to Archean "melt depletion ages" (T_{MA}, determined by using the measured Re/Os ratio of the sample to calculate when the $^{187}Os/^{188}Os$ matched primitive upper mantle; c.f. Shirey and Walker 1998; this is completely analogous to the Sm-Nd model age) of 2.00–3.72 Ga (Wu et al. 2006). The Tieling kimberlites also contain highly serpentinized peridotite xenoliths that give T_{RD} ages older than the chromites (1.9–2.3 Ga). However, the age of Tieling kimberlite emplacement is unknown, thus ages of the lithospheric mantle before the thinning are still not well constrained.

This study focuses on mantle peridotite xenoliths and xenocrysts from the early Paleozoic Mengyin and Fuxian diamondiferous kimberlites from the North China Craton, and mantle xenoliths from Paleozoic-age barren kimberlites and Mesozoic basalts from Dahongshan, Ningyuan, and Fangcheng on the South China and North China Cratons (Fig. 1). We report major and trace element chemistry, including PGEs, Re–Os isotope systematics, and Sr-Nd isotopes on samples representing all the localities. The purpose is to characterize the chemical and isotopic compositions of the lithospheric mantle beneath eastern China, to constrain the age of the lithospheric mantle that existed during the Paleozoic and Mesozoic, and to address the mechanism for lithospheric thinning.

Geological background

Eastern China comprises several tectonic units, from south to north, the South China Craton, the Qilian-Qinling-Dabie-Sulu Orogenic Belt, the North China Craton and the eastern Central Asia Orogenic Belt (Fig. 1). These units amalgamated during the Late Paleozoic–Early Mesozoic. A brief description of the tectonic evolution is given below.

South China Craton

The South China Craton comprises the Yangtze Block and the Cathaysia Block (Fig. 1). The Yangtze Block is one of the three old continents in China. Its basement formed dominantly in the Proterozoic (1.85–0.85 Ga) and is covered by Phanerozoic sedimentary rocks (Zhang et al. 1994). However, recent work on zircon U-Pb ages and Hf isotopes of gneiss xenoliths in lamproite diatremes from Proterozoic terrains indicates a widespread presence of Archean basement with zircon ages of 2.5–2.6 and 2.8–2.9 Ga and Hf model ages of 2.6–3.5 Ga (Zheng et al. 2006c). There are three kimberlite and/or lamproite fields: the Dahongshan barren kimberlite-lamproite field in Hubei Province, the Ningxiang diamond-bearing lamproite field in Hunan Province, and the Zhengyuan diamond-bearing lamproite field in Guizhou Province (Fig. 1). The Dahongshan kimberlite-lamproite field comprises *ca.* 100 small kimberlite or lamproite vents or dikes. These dikes intruded Sinian-Ordovician carbonates and shales (Liu and Zhao 1991). Ten irregular kimberlite vents outcrop near Pengjiabang village where the xenolith of this study was collected (Zhang et al. 2001). The kimberlite breccias are composed of porphyritic phlogopite and olivine macrocrysts and

aphanitic matrix as well as wallrock fragments. The aphanitic kimberlite in this area gave a K-Ar whole-rock age of 326 Ma (Liu et al. 1993).

The Cathaysia Block (Fig. 1) comprises the Western and Eastern Cathaysia, whose boundary broadly corresponds to the boundary between Mesozoic S-type granites to the northwest and I-type granites to the southeast (Li et al. 2003). The oldest crustal component of western Cathaysia is represented by 2.5 Ga inherited zircons in Mesozoic granites (Li et al. 1989). The Cathaysia Block underwent a series of reworking events in the Neoproterozoic (Li et al. 1997, 1999, 2000; Chen and Jahn 1998; Chen et al. 1991). However, there are no reports of Paleozoic magmatism in this block.

In the Daoxian–Ningyuan region of Hunan Province (Fig. 1), Mesozoic basalts erupted at 151–131 Ma along the Ningyuan-Jianghua fault (Wang 1991). Some xenoliths in this study are from the Ningyuan basalt field, where, in the Anyuan area of Jiangxi Province, there exists more than 20 Eocene lamprophyre pipes. The pipes explosively intruded into Late Jurassic rhyolites (Zheng et al. 2004) and contain abundant peridotite xenoliths and megacrysts of augite, amphibole and phlogopite. Neogene xenolith-bearing basalts are widespread in the eastern Cathaysia, but rare in the western Cathaysia.

North China Craton

The North China Craton (Fig. 1) comprises Eastern and Western Blocks and the intervening Trans-North China Orogen (Zhao et al. 2000, 2001, 2005; Li et al. 2001; Gao et al. 2002; Wang et al. 2004). The basement of the Eastern Block consists primarily of Archean tonalitic, trondhjemitic and granodioritic (TTG) gneisses and granitoids, with rafts of Archean granitic gneisses and supracrustal rocks (Zhao et al. 2000, 2001). The Western Block is composed of Late Archean to Paleoproterozoic metasedimentary belts (Li et al. 2001; Zhao et al. 2000, 2005), which mainly consists of granulite-facies TTG gneisses and charnockites. The Trans-North China Orogen (Zhao et al. 2001; Gao et al. 2002), roughly north-south trending across the North China Craton, consists of a series of 2.5–2.7 Ga greenschist-amphibolite to granulite facies terrains (Zhao et al. 2000, 2001, 2005; Kröner et al. 1988). This Orogen was formed by the collision between the Eastern and Western Blocks at ~1.8 Ga (Zhao et al. 2000, 2001), representing the final cratonization event.

The North China Craton experienced widespread tectono-thermal reactivation since the Phanerozoic, manifested by emplacement of Early Paleozoic kimberlites, extensive Late Mesozoic basaltic rocks and granites, and Cenozoic alkali basalts (e.g., Fan et al. 2000; Zhang et al. 2002, 2004; Wu et al. 2005). Ordovician diamondiferous kimberlites occur mainly in Mengyin County, Shandong Province, and Fuxian, Tieling and Huairen Counties, Liaoning Province (Fig. 1) (Dobbs et al. 1994; Chi and Lu 1996). Kimberlite-borne xenocrystic minerals and xenoliths having refractory compositions indicate cool geotherms (36–40 mW/m^2) and thick lithosphere (~200 km) at the time of emplacement (Menzies et al. 1993; Griffin et al. 1998). These features are characteristics of lithospheric mantle beneath Archean cratons worldwide and indicate that an Archean lithospheric keel existed beneath the Eastern Block at least until the Paleozoic (Zheng et al. 2006b). In contrast, mantle xenoliths from Cenozoic basalts record shallower and hotter lithospheric mantle, predominantly composed of fertile spinel peridotites (Fan et al. 2000; Rudnick et al. 2004), consistent with an average present-day surface heat flow of 60 mW/m^2 (Hu et al. 2000) and thin lithosphere of 80–60 km beneath the Eastern Block (Yuan 1996; Griffin et al. 1998; Chen et al. 2006). This suggests that a considerable amount of Archean lithosphere has been lost or transformed to relatively young lithosphere.

Xenolith localities and petrology

The xenoliths investigated in this study are from five localities (Fig. 1). On the South China Craton they are (1) the Early Carboniferous Dahongshan kimberlite–lamproite field on the northern margin of the Yangtze Block (Liu and Zhao 1991; Zhang et al. 2001); (2) the Late Jurassic–Early Cretaceous Ningyuan-Diaoxian basaltic field on the Cathaysian Block. On the North China Cration they are (3) the Mid-Ordovician Fuxian kimberlite field (Chi and Lu 1996; Griffin et al. 1998; Zhang and Yang 2007); (4) the Mid-Ordovician Mengyin kimberlite field (Dobbs et al. 1994; Lu et al. 1998); and (5) the Early Cretaceous Fangcheng basaltic field (Zhang et al. 2002; Zhang and Sun 2002).

South China Craton

The xenolith from the Dahongshan kimberlite field (Fig. 1) is a fresh garnet lherzolite, composed of Ol (60%), Opx (15%), Cpx (15%), and Gt (10%). It has a granuloblastic texture, with some features of deformation and recrystallization, such as kink bands in olivine and orthopyroxene and triple junctions between olivine and pyroxene. Most of the constituent minerals are 0.1–3 mm across. Olivines often possess small fractures and orthopyroxenes are colorless with well-developed cleavages. A few orthopyroxenes show poikilitic textures and enclose olivine and clinopyroxene. Clinopyroxene is light emerald diopside, small in grain size, and homogeneously scattered. Garnets are

relatively large (dominantly 1–5 mm) and red-purple. Some garnets have kelyphitic rims composed of tiny pyroxenes and spinels. This xenolith appears to represent the residue after low degree partial melting of the upper mantle, which was refertilized by later stage mantle metasomatism, as indicated by high proportions of garnet and enrichment of incompatible trace elements (Zhang et al. 2001).

The Ningyuan–Daoxian basaltic field (Fig. 1) contains abundant spinel facies peridotite and gabbro xenoliths and rare granulitic xenoliths (Wang et al. 1997). The peridotites in this study were collected from the Ningyuan basalts. All of these spinel-facies xenoliths are angular, with an average size of 3 cm across, and have relatively low olivine (50–60%) and high clinopyroxene (10–15%) contents. Most of the peridotites have a porphyroclastic microstructure (Zheng et al. 2004), indicating strong deformation of the sub-continental lithospheric mantle along the Ningyuan–Jianghua fault. The olivines and pyroxenes contain abundant fluid inclusions, providing direct evidence for the presence of significant volume of a fluid phase. Four porphyroclastic spinel lherzolites were selected for analyses (Table 1).

North China Craton

Fuxian kimberlites (Fig. 1) erupted through the Archean (2.9–2.5 Ga) Anshan terrain (Chi and Lu 1996). The peridotite xenoliths examined here, all from Pipe 50, have coarse granular textures and are strongly serpentinized and carbonated, as reflected by high loss on ignition values (15.3–25.6 wt%) and high CaO contents (7–18 wt%). The freshest sample (L50–2003) is a garnet bearing peridotite containing kelyphitic pyrope (as high as 5%) and olivine relicts with Fo as high as 92 and Mg# up to 90.6. The more altered peridotites contain small amounts of visible sulfides (Table 1). These samples have relatively low Mg# (85–89) compared to typical coarse-granular peridotites from other Archean cratons (Mg# = 92–93) (Boyd 1989; Gao et al. 2002). Although the absence of primary mineral phases makes it impossible to determine P-T conditions, the presence of garnet in some xenoliths suggests minimum derivation from depths greater than 75 km based on typical cratonic geotherms (Menzies and Xu 1998).

Fuxian sample F50–9229 is a composite spinel lherzolite xenolith interlayered with garnet granulite composed of garnet (30%), pyroxene (15%), plagioclase (50%) and Ba-bearing feldspar (5%) (Zhang 2006). This composite xenolith is thus derived from the crust-mantle transition zone. L42–13 is a serpentinized olivine megacryst collected from Pipe 42. Chromite separate (F50–01) is from kimberlites of Pipe 50 and is studied for comparison.

Mengyin diamondiferous kimberlites (Fig. 1) erupted through the Archean to Paleoproterozoic (2.7–2.3 Ga) Taishan terrain (Chi and Lu 1996). The garnet-bearing peridotite xenoliths have porphyroclastic textures, while a spinel peridotite xenolith has a coarse-granular texture. All were collected from Pipe Shengli 1, which erupted at 460–465 Ma based on U-Pb dating of perovskite (Dobbs et al. 1994) and Ar-Ar dating of a phlogopite megacryst (Zhang and Yang 2007). Like the Fuxian xenoliths, these peridotites are strongly serpentinized, and no primary minerals are preserved. They have high Mg# (89.4–91.8, Table 2), but are lower than the peridotite (92.2) reported in Gao et al. (2002). There are no obvious differences in Mg# between the porphyroclastic and coarse-granular peridotites, distinctive from the porphyroclastic and coarse-granular peridotites from other cratons (Smith and Boyd 1987).

An amphibole-bearing pyroxenite (Sv1b-16) from Mengyin is a macrocrystic xenolith with a cumulate texture. It is dominantly composed of coarse-grained (0.5–1.5 cm) clinopyroxene (90% augite) with minor amphibole and plagioclase, and represents a cumulate of ancient basaltic magma underplated in the crust-mantle boundary.

The Fangcheng basalts (Fig. 1) erupted at ~125 Ma (Zhang et al. 2002) and contain spinel-facies ultramafic xenoliths, occurring as olivine clinopyroxenites and websterites, and range in size from 2–8 cm in diameter. They are mainly composed of clinopyroxene and orthopyroxene with minor olivine, spinel and plagioclase. Clinopyroxenes and sometimes orthopyroxenes in these pyroxenite xenoliths occur as large crystals (2–6 mm) and show cumulate textures (Zhang et al. 2007). Olivine, spinel, and occasionally feldspar occur as small interstitial grains among clinopyroxenes. Three pyroxenite xenoliths were selected for this study (Table 1).

Analytical methods

Major and trace element analyses

Whole rocks were powdered with an agate mill. Major oxides (Table 2) were obtained with a Phillips PW 2400 sequential X-ray fluorescence spectrometer at the University of Hong Kong (HKU). Fused glass disks were used for XRF major oxide determinations. The analytical precision is better than ±2%. Trace elements (Table 2) were determined with a VG Elemental Plasma-Quad 3 ICP-MS at HKU after normal sample digestion using ultra-pure acid (HF-HNO_3). Detailed sample preparation procedures are available in Zhang et al. (2001). A blank solution was prepared and the total procedural blanks were <50 ng for all the trace elements reported in this paper. Two standards (BEN, BHVO-1) were prepared using the same procedure to monitor the analytical reproducibility. Discrepancies between triplicate analyses are less than ±5% for all elements.

Table 1 Sample description of mantle xenoliths entrained in Paleozoic kimberlites and Mesozoic basalts on the North China Craton and South China Block

Location	Sample	Rock type	Description
South China Craton	Early Carboniferous (326 Ma) Dahongshan kimberlites		
	DHS	Garnet lherzolite	Fresh granular garnet lherzolite
	Late Jurassic–Early Cretaceous (151 ~ 131 Ma) Ningyuan basalts		
	NY-G1	Spinel lherzolite	Fresh spinel porphyroclastic lherzolite
	NY-G2	Spinel lherzolite	Fresh spinel porphyroclastic lherzolite
	NY-G3	Spinel lherzolite	Fresh spinel porphyroclastic lherzolite
	NY-G4	Spinel lherzolite	Fresh spinel porphyroclastic lherzolite
North China Craton	Mid-Ordovician (465 Ma) Fuxian kimberlites		
	L50-2003	Garnet lherzolite	Kelyphite pyrope-bearing serpentinized peridotite with few fresh olivine relicts, pyrope can be as high as 5% and up to 7 mm.
	LN-9830	Garnet lherzolite	Garnet-bearing serpentinized peridotite, fresh Cr-pyrope
	F50-9254	Spinel peridotite with sulfides	Highly serpentinized peridotite, rare sulphide and spinel
	F50-9270	Peridotite with sulfides	Highly serpentinized peridotite, rare sulphide, both spinel and garnet have not been found
	F50-9274	Peridotite with sulfides	Highly serpentinized peridotite, rare sulphide, both spinel and garnet have not been found
	F50-9281	Spinel peridotite with sulfides	Highly serpentinized peridotite, lots of sulphides and rare spinel
	F50-9229	Composite xenolith	Spinel lherzolite interlayered with garnet granulite composed of garnet, pyroxene and plagioclase
	L42-13	Olivine megacryst	Single serpentinized olivine megacryst from Pipe 42, Fuxian kimberlite field
	F50-01	Chromite separate	Chromite separate from Pipe 50, Fuxian kimberlite field
	Mid-Ordovician (465 Ma) Mengyin kimberlites		
	SD-9804	Garnet lherzolite	Garnet-bearing serpentinized peridotite
	SL-2001	Garnet lherzolite	Garnet-bearing serpentinized lherzolite
	Sv1b-12	Garnet lherzolite	Garnet-bearing serpentinized lherzolite
	Sv1b-11	Spinel peridotite	Spinel-bearing serpentinized peridotite
	Sv1b-16	Pyroxenite	Amphibole-bearing macrocrystic clinopyroxenite with grain sizes in a range of 0.5-1.5 cm, cpx is augitic composition
	Early Cretaceous (125 Ma) Fangcheng basalts		
	FC6-1-2	Pyroxenite	Olivine clinopyroxenite
	FC6-2-2	Pyroxenite	Olivine clinopyroxenite
	FC25-2	Pyroxenite	Clinopyroxenite

Emplacement ages of 465 Ma for the Fuxian and Mengyin kimberlites are the Ar-Ar ages of phlogopite megacrysts (Zhang and Yang 2007)

Platinum group elements (PGE) and Au

Platinum group elements and Au (Table 2) were also measured with the ICP-MS at HKU after a pre-concentration by Ni-sulfide fire assay and the Te co-precipitation (Sun et al. 1993; Zhou 1994). Mass 108 (^{108}Pd) and mass 105 (^{40}Ar^{65}Cu and ^{105}Pd) were measured in order to evaluate the contribution of ^{40}Ar^{65}Cu, so that ^{63}Cu^{40}Ar interference with ^{103}Rh could be evaluated. Standard materials WPR-1 and TDB-1 were analyzed and analytical uncertainties were better than ±15% for Ru and Rh, and ±10% for Ir, Pd and Pt (Zhou et al. 2000).

Sr-Nd isotopic determination

For Sr-Nd isotopic analyses, sample powders were spiked with mixed isotope tracers (^{87}Rb-^{84}Sr and ^{149}Sm-^{150}Nd), dissolved in Teflon capsules with HF+HNO_3 acid, and separated by conventional cation-exchange techniques.

Table 2 Major oxide, trace element concentration, PGE and Au abundances of mantle xenoliths entrained in the Paleozoic kimberlites and Mesozoic basalts on the North China Craton and South China Craton

Sample	DHS	NY-G1	NY-G2	NY-G3	NY-G4	L50-2003	LN-9830	F50-9254	F50-9270	F50-9274	F50-9281	F50-9229	L42-13	F50-01	SD-9804	SL-2001	Sv1b-11	Sv1b-12	Sv1b-16	FC6-1-2	FC6-2-2	FC25-2
Major oxide (wt%)																						
SiO_2	44.2	44.8	46.9	45.8	45.4	53.3	42.7	30.9	28.7	43.8	42.7	40.7			39.6	39.1	38.1	39.7	46.9	45.6	45.9	52.6
TiO_2	0.13	0.14	0.13	0.11	0.12	0.09	0.05	0.01	0.02	0.12	0.02	0.37			0.27	0.05	0.11	0.09	0.37	0.48	0.49	0.29
Al_2O_3	2.66	3.63	3.55	3.24	3.09	2.21	1.50	1.02	0.69	0.67	1.11	16.8			0.67	0.70	1.84	1.06	5.34	2.81	3.03	2.11
Cr_2O_3	0.44	0.33	0.34	0.33	0.35	0.60	0.47	0.53	0.50	0.13	0.32	0.04			0.38	0.49	1.36	0.43				
Fe_2O_3	8.14	9.26	9.34	9.53	9.66	6.03	5.43	5.39	5.30	7.70	6.21	10.9			7.05	8.65	7.95	6.49	7.11	9.15	9.05	6.56
MnO	0.12	0.13	0.12	0.13	0.13	0.05	0.17	0.48	0.47	0.07	0.13	0.05			0.06	0.05	0.08	0.10	0.22	0.20	0.13	0.14
MgO	40.9	37.3	35.1	36.6	36.9	29.2	21.3	20.5	22.2	22.4	20.6	18.1			38.1	36.7	36.4	36.6	14.2	24.1	24.5	20.2
NiO	0.33	0.25	0.26	0.27	0.27	0.24	0.11	0.13	0.13	0.12	0.17	0.04			0.32	0.30	0.36	0.39				
CaO	2.82	4.03	3.45	3.59	3.80	0.93	10.5	18.1	16.3	6.96	13.3	2.13			0.44	0.54	0.61	1.13	22.4	14.6	13.8	16.7
Na_2O	0.12	0.21	0.27	0.25	0.22	0.09	0.07	0.11	0.08	0.26	0.06	0.81			0.07	0.04	0.04	0.03	0.45	0.18	0.20	0.16
K_2O	0.05											1.55							0.44	0.03	0.06	0.05
LOI						7.16	17.5	22.8	25.6	17.8	15.3	8.50			13.0	13.3	13.0	13.9	2.68	3.29	2.86	1.40
Mg#	90.9	88.9	88.1	88.4	88.3	90.6	88.6	88.3	89.2	85.2	86.8	76.7			91.5	89.4	90.1	91.8	79.8	83.7	84.1	85.8
Trace element concentration (ppm)																						
Li		8.32	15.1	7.15	6.04	36.47	59.9		21.2			420			51.0	86.7	35.0	48.2	23.2			
Be		0.08	0.12	0.10	0.11	1.04	1.27		1.53			4.29			1.41	0.56	0.95	0.45	0.63			
Cs		0.17	1.64	0.89	0.92	3.53	2.16		2.66			12.3			0.91	0.88	0.81	0.98	1.40			
Ba	55.4	0.96	1.58	1.73	0.39	13.2	78.9		55.1			717			30.4	48.2	135	11.5	1011	81.0	103	25.0
Rb	2.49	0.62	1.06	0.88	0.76	3.15	1.6		1.90			29.0			3.94	2.30	5.9	1.64	19.0	1.70	1.90	0.70
Th		0.09	0.20	0.03	0.04	0.21	0.47		0.16			0.33			0.30	0.96	0.67	1.34	1.47	2.40	2.30	1.60
Nb	1.33	0.37	1.57	0.43	0.58	3.04	5.54		1.43			3.19			13.9	9.99	17.7	22.2	2.51	1.20	0.70	0.30
Ta		0.03	0.09	0.02	0.02	0.15	0.22		0.06			0.13			0.31	0.46	0.55	0.58	0.09	1.00	0.30	0.40
La	2.49	0.44	1.57	0.35	0.38	39.6	41.7		48.4			2.94			16.7	25.7	19.4	36.9	47.8	12.1	15.6	9.49
Ce	3.88	1.14	3.24	0.88	0.96	64.5	96.7		96.6			5.93			16.4	34.5	24.3	50.1	110	33.7	39.6	28.6
Pr	0.36	0.18	0.40	0.14	0.15	5.28	12.4		11.5			0.65			1.30	3.09	2.23	4.57	16.0	5.14	5.89	4.49
Sr	21.5	22.4	26.30	20.2	18.9	88.0	172		142			350			32.3	52.7	86.0	66.9	330	166	192	180
Nd	1.04	0.95	1.74	0.69	0.90	14.8	52.6		46.5			2.63			4.51	10.7	7.79	15.6	77.5	25.8	29.0	22.4
Zr	2.17	6.69	14.4	5.68	7.47	7.16	9.74		5.51			18.4			20.0	12.6	23.1	31.7	66.7	40.0	53.0	27.0
Hf		0.18	0.30	0.13	0.18	0.18	0.18		0.14			0.47			0.52	0.47	0.55	0.82	2.39	3.80	3.20	2.00
Sm	0.12	0.33	0.44	0.25	0.30	1.07	10.6		8.03			0.61			0.69	1.96	1.16	1.98	14.5	5.98	6.55	5.66
Eu	0.04	0.11	0.15	0.09	0.10	0.25	2.44		1.93			0.38			0.19	0.45	0.30	0.53	3.60	1.87	1.96	1.61
Gd	0.17	0.43	0.52	0.33	0.38	0.55	4.51		4.18			0.72			0.49	1.12	0.72	1.42	9.41	5.40	5.45	4.39
Tb	0.03	0.08	0.09	0.06	0.07	0.06	0.38		0.39			0.12			0.06	0.13	0.08	0.13	0.93	0.75	0.80	0.59

Table 2 continued

Sample	DHS	NY-G1	NY-G2	NY-G3	NY-G4	L50-2003	LN-9830	F50-9254	F50-9270	F50-9274	F50-9281	F50-9229	L42-13	F50-01	SD-9804	SL-2001	Sv1b-11	Sv1b-12	Sv1b-16	FC6-1-2	FC6-2-2	FC25-2
Dy	0.27	0.55	0.62	0.43	0.49	0.27	1.34		1.50			0.81			0.32	0.44	0.37	0.59	4.01	4.06	4.16	2.86
Ho	0.06	0.12	0.13	0.10	0.11	0.05	0.18		0.20			0.17			0.05	0.06	0.06	0.09	0.59	0.62	0.61	0.45
Er	0.21	0.35	0.40	0.29	0.32	0.09	0.34		0.35			0.49			0.11	0.09	0.13	0.20	1.25	1.24	1.23	0.93
Tm	0.03	0.05	0.06	0.05	0.05	0.01	0.03		0.03			0.07			0.01	0.01	0.02	0.02	0.15	0.15	0.16	0.12
Yb	0.24	0.38	0.44	0.33	0.35	0.06	0.16		0.15			0.50			0.08	0.05	0.08	0.14	0.72	0.93	1.04	0.70
Lu	0.04	0.05	0.06	0.05	0.05	0.01	0.02		0.02			0.07			0.01	0.01	0.01	0.02	0.08	0.14	0.16	0.10
Y	1.55	3.63	3.86	3.00	3.23	1.24	5.90		5.20			4.81			1.61	1.78	1.71	2.63	14.9	16.7	16.9	13.8
Sc		18.6	16.9	15.7	15.6	4.30	28.0		46.6			6.6			3.6	3.7	4.1	20.3	64.6	29.0	25.0	28.0
ΣREE	9.0	5.2	9.9	4.0	4.6	127	223		220			16.1			40.9	78.3	56.7	112	287	98	112	82
$(La/Yb)_P$	7.4	0.8	2.6	0.8	0.8	474	187		232			4.2			150	369	174	189	47.6	9.3	10.8	9.7
PGE and Au abundance (ppb)																						
Ir	3.60	3.37	4.03	2.62	3.65	3.47	3.65	4.81	3.35	4.50	8.59	0.17	0.39	52.2	2.44	4.55	4.15	3.42				
Ru	4.86	5.80	7.26	4.88	6.70	7.41	7.58	5.70	6.19	5.44	16.6	0.28	0.71	41.1	3.66	5.97	8.68	4.15				
Rh	1.36	1.69	1.79	1.13	1.28	1.92	2.10	0.89	0.86	0.64	2.59	0.11	0.34	5.68	0.56	0.71	1.97	0.60				
Pt	9.66	6.87	8.87	6.59	8.28	3.67	2.71	3.56	2.05	2.48	7.01	1.44	1.75	17.8	3.25	3.52	10.3	2.08				
Pd	9.18	6.75	8.65	6.62	8.32	4.11	2.86	2.93	2.72	2.68	4.30	2.21	2.79	5.65	4.01	3.25	4.70	2.70				
Au	11.3	4.10	7.15	5.40	5.27	5.57	2.98	3.03	4.02	4.17	1.70	5.83	6.16	16.9	4.56	9.31	3.81	3.24				
Pd/Ir	2.55	2.00	2.15	2.53	2.28	1.18	0.78	0.61	0.81	0.60	0.50	13.0	7.15	0.11	1.64	0.71	1.13	0.79				

Major oxides for Mengyin and Fuxian kimberlite-borne xenoliths were recalculated to 100%. Blank means that the analysis is not available. Data of sample DHS are taken from Zhang et al. (2001). ΣREE is the total concentration of the REE, $(La/Yb)_P$ is the Primotive Mantle-normalized La/Yb ratio (McDonough and Sun 1995)

LOI Loss On Ignition, *Mg#* 100Mg/(Mg + Fe^{3+}) mole fraction

Isotopic measurements were performed on the VG-354 mass-spectrometer at the Institute of Geology and Geophysics, Chinese Academy of Sciences. The mass fractionation corrections for Sr and Nd isotopic ratios were based on $^{86}Sr/^{88}Sr = 0.1194$ and $^{146}Nd/^{144}Nd = 0.7219$, respectively. The detailed sample preparation and analytical procedures are reported in Zhang et al. (2001). Over the period of analytical work, repeat analyses yielded an $^{87}Sr/^{86}Sr$ ratio of 0.710230 ±40 for the NBS-987 Sr standard and a $^{143}Nd/^{144}Nd$ ratio of 0.511845 ± 12 for the La Jolla standard. Total blanks for Rb, Sr, Sm and Nd were less than 100 pg. The results are given in Table 3.

Re–Os isotopic measurements

Sample preparation and sparging procedures for Os isotope measurements were based on Ravizza and Pyle (1997), Hassler et al. (2000), and Schoenberg and Kramers (2000). Re and Os concentrations and Os isotopes were measured on a VG Axiom MC-ICPMS at the Lamont-Doherty Earth Observatory by static multi-collection.

For Re analyses, 1 g of sample powder and ^{185}Re spike solution was weighed into a 60 ml Teflon screw cap beaker. Concentrated HF+HNO_3 (24 ml) was added to dissolve silicates. The beaker was sealed and left on the hotplate at 120°C for 2 days. After drying, 2 ml of concentrated HNO_3 was added expel HF, and dried down. Concentrated HCl (10 ml) was added and the sample remained on a hotplate at 120°C overnight. The clear solution was dried down carefully to avoid complete dryness and 2 ml of concentrated HNO_3 was added to form soluble nitrates. The solution was dried down carefully and dissolved in 10 ml 0.5 N HNO_3, then centrifuged to separate any solid residue. About 1 ml of AG1-X8 resin was slurried into HDPE columns for Re separation. The column was washed four times with 2 ml 4 N HNO_3. After conditioning the resin twice with 1 ml 0.5 N HNO_3 and once with 5 ml 0.5 N HNO_3, the sample was loaded and subsequently rinsed three times with each 5 ml 0.5 N HNO_3. Rhenium was eluted three times with 5 ml 4 N HNO_3 and the solution was collected in a clean 20 ml Teflon screw cap vial. Prior to analysis, the solution was dried down carefully at 90°C and dissolved again in 40 µl 4 N HNO_3. This solution was then transferred to a clean centrifuge vial and diluted to 1 ml with ultraclean water. Instrumental mass fractionation was monitored by measurement of a Re standard solution.

For Os isotopes, 5 g of sample powder was weighed into a clean ceramic crucible capped with a ceramic lid and spiked with ^{190}Os. The crucible was placed on a warm (60°C) oven to dry the spike solution. The possibility of volatilization of the Os spike at this stage could result in some high estimates of Os concentrations. However, this would be manifested in model ages that are too old, which we do not see in the results. The dry powder and spike were thoroughly mixed with 20 g borax, 2 g nickel powder and 1 g of sulfur powder. This mixture was fused for an hour in a muffle furnace at 11,00°C. After cooling, the crucible was crushed, and NiS beads were collected and dissolved in 6 N HCl on a hotplate at 200°C, in an Erlenmeyer flask covered with a Teflon lid. The green-colored solution was filtered through 0.45-µm cellulose filter paper, and the insoluble residue with the Os was collected. The filter paper containing the Os concentrate was digested with 5 ml of 16 N nitric acid in an Os sparging apparatus connected to the MC-ICPMS. The oxidized OsO_4 vapor was directly sparged into the torch by an Ar gas stream where it is ionized to Os^+ and measured. Total procedural blanks did not exceed 2 pg for Re and 3 pg for Os. Blank corrections were made to all samples using an average Re blank of 1 pg and Os blank of 2 pg. The measured isotope ratios were corrected for mass fractionation using $^{189}Os/^{188}Os = 1.2212$. Replicate analyses by sparging of an in-house standard solution from Spex averaged $^{187}Os/^{188}Os = 0.10638 \pm 0.00077$ (2σ external reproducibility, $n = 22$). This is half the error reported by Hassler et al. (2000) for sparge analyses using a Finnegan Element single collector instrument. The accuracy of the measurements is verified by comparison of analyses on sample F50–9270 (Table 4), performed in this study and by Gao et al. (2002), which gave identical $^{187}Os/^{188}Os$ ratios (0.11015 ± 11 and 0.11011 ± 11, respectively). However, replicate Re and Os concentrations vary beyond analytical uncertainty (2%), indicating heterogeneity of the whole rock or the so-called "nugget effect", since the concentrations were measured on powder aliquots. In addition, imperfect dissolution of Re-rich phases and some volatilization of the Os spike during the digestion step could contribute to imprecision of the concentrations.

Analytical results

Dahongshan garnet lherzolite xenolith

The Dahongshan garnet lherzolite xenolith has relatively high Al_2O_3 (2.7%) and CaO (2.8%), higher than average global kimberlite-borne garnet lherzolites from old cratonic lithospheric mantle (~1.3 and 0.8%, respectively; McDonough 1990). It shows a V-shaped REE pattern (Figs. 2, 3), that is, with low MREEs compared to LREE and HREE. PGE and Os concentrations are very close to primitive mantle abundances (Barnes et al. 1988) but shows enrichment of Pd and Au (Fig. 4). The Pd/Ir ratio (2.55) is higher than that for garnet lherzolite from Matsoku kimberlites

Table 3 Sr-Nd isotopic ratios of mantle xenoliths from the Paleozoic kimberlites and Mesozoic basalts on the North China Craton and South China Craton

Location	Sample	Rock	$^{87}Rb/^{86}Sr$	$^{87}Sr/^{86}Sr$	± 2σ	$(^{87}Sr/^{86}Sr)_i$	$\varepsilon_{Sr(t)}$	$^{147}Sm/^{144}Nd$	$^{143}Nd/^{144}Nd$	± 2σ	$(^{143}Nd/^{144}Nd)_i$	$\varepsilon_{Nd(t)}$
South China Craton	Early Carboniferous (326 Ma) Dahongshan kimberlites											
	DHS	Garnet lherzolite	0.3344	0.706614	10	0.705060	13.57	–	–	–	–	–
	Late Jurassic–Early Cretaceous (151 ~ 131 Ma) Ningyuan basalts											
	NY-G1	Spinel lherzolite	0.0799	0.705141	20	0.704981	9.2	0.2100	0.513341	10	0.513147	13.5
	NY-G2	Spinel lherzolite	0.1167	0.705045	29	0.704811	6.8	0.1529	0.513188	8	0.513047	11.5
	NY-G3	Spinel lherzolite	0.1256	0.705049	15	0.704797	6.6	0.2190	0.513319	13	0.513117	12.9
	NY-G4	Spinel lherzolite	0.1163	0.705055	10	0.704822	7.0	0.2015	0.513206	12	0.513020	11.0
North China Craton	Mid-Ordovician (465 Ma) Fuxian kimberlites											
	L50-2003	Garnet lherzolite	0.1147	0.715043	20	0.714283	147	0.0450	0.512090	12	0.511953	−1.7
	LN-9830	Garnet lherzolite	0.0503	0.719958	68	0.719625	223	0.1073	0.512155	7	0.511828	−4.1
	F50-9254	Spinel peridotite	0.0183	0.713809	16	0.713688	139	0.1037	0.512138	6	0.511822	−4.2
	F50-9270	Peridotite	0.0575	0.713983	14	0.713602	137	0.0999	0.512155	7	0.511851	−3.7
	F50-9274	Peridotite	0.0017	0.712739	17	0.712728	125	0.0973	0.512148	7	0.511852	−3.7
	F50-9281	Spinel peridotite	0.0110	0.712576	28	0.712503	122	0.0802	0.512097	8	0.511853	−3.6
	F50-9229	Composite xenolith	0.2650	0.710423	18	0.708667	67.2	0.1485	0.512503	8	0.512051	0.2
	Mid-Ordovician (465 Ma) Mengyin kimberlites											
	SD-9804	Garnet lherzolite	0.4297	0.710389	18	0.707542	51.2	0.0954	0.512297	9	0.512006	−0.6
	SL-2001	Garnet lherzolite	0.2023	0.708805	12	0.707465	50.1	0.1069	0.512393	7	0.512067	0.6
	Sv1b-12	Garnet lherzolite	0.0861	0.708666	16	0.706016	59.1	0.0769	0.512264	9	0.512018	−0.2
	Sv1b-11	Spinel peridotite	0.2211	0.707481	15	0.703096	29.5	0.0889	0.512289	8	0.512030	−0.4
	Sv1b-16	Pyroxenite	0.2447	0.706358	14	0.704737	11.3	0.2944	0.511637	8	0.510740	−25.4
	Early Cretaceous (125 Ma) Fangcheng basalts											
	FC6-1-2	Pyroxenite	0.1630	0.710037	11	0.709759	76.6	0.1518	0.511990	6	0.511871	−12.0
	FC6-2-2	Pyroxenite	0.0346	0.710115	17	0.710056	81.0	0.1367	0.511978	7	0.511871	−12.0
	FC25-2	Pyroxenite	0.0050	0.709802	19	0.709793	77.3	0.1279	0.511949	12	0.511849	−12.4

Chondrite Uniform Reservoir (CHUR) values ($^{87}Rb/^{86}Sr$ = 0.0847, $^{87}Sr/^{86}Sr$ = 0.7045, $^{147}Sm/^{144}Nd$ = 0.1967, $^{143}Nd/^{144}Nd$ = 0.512638) are used for the calculation. $\lambda_{Rb} = 1.42 \times 10^{-11}$ $year^{-1}$; $\lambda_{Sm} = 6.54 \times 10^{-12}$ $year^{-1}$ (Steiger and Jäger 1977; Lugmair and Marti 1978). Emplacement ages of the Paleozoic kimberlites and Mesozoic basalts were used to calculate the initial isotopic ratios. For samples from Ningyuan, the average age of 141 Ma was used. Data of sample DHS are taken from Zhang et al. (2001)

Table 4 Re–Os isotopic compositions of mantle xenoliths from the Paleozoic kimberlites and Mesozoic basalts on the North China Craton and South China Craton

Location	Sample	Rock	Re (ppb)	Os (ppb)	$^{187}Re/^{188}Os$	$^{187}Os/^{188}Os$	± 2σ	$(^{187}Os/^{188}Os)_i$	γ_{Os}	T_{MA} (Ga)	T_{RD} (Ga)
South China Craton	Early Carboniferous (326 Ma) Dahongshan kimberlites										
	DHS	Garnet lherzolite	0.3078	4.0652	0.3641	0.12404	15	0.12205	−4.08	4.66	1.04
	Late Jurassic–Early Cretaceous (151–131 Ma) Ningyuan basalts										
	NY-G1	Spinel lherzolite	0.2293	3.3616	0.3280	0.12553	20	0.12476	−2.98	2.28	0.67
	NY-G2	Spinel lherzolite	0.9834	3.9435	1.1991	0.12519	12	0.12238	−4.83	future	0.99
	NY-G3	Spinel lherzolite	0.1266	2.0788	0.2928	0.12311	16	0.12242	−4.79	2.72	0.99
	NY-G4	Spinel lherzolite	0.2583	3.7695	0.3295	0.12367	22	0.12290	−4.42	3.34	0.92
North China Craton	Mid-Ordovician (465 Ma) Fuxian kimberlites										
	L50-2003	Garnet lherzolite	0.1190	3.2597	0.1756	0.11582	12	0.11445	−9.33	3.13	2.06
	LN-9830	Garnet lherzolite	0.1002	2.3203	0.2077	0.10878	16	0.10716	−15.11	5.31	3.03
	F50-9254	Spinel peridotite	0.0323	3.5555	0.0437	0.10717	17	0.10683	−15.37	3.36	3.08
	F50-9270	Peridotite	0.0279	3.4504	0.0389	0.11015	11	0.10984	−12.98	2.89	2.68
	F50-9270*	Peridotite	0.0150	1.2000	0.0620	0.11011	11	0.10963	−13.15	3.07	2.70
	F50-9271*	Peridotite	0.0260	1.7240	0.0705	0.10919	31	0.10864	−13.94	3.14	2.68
	F50-9274	Peridotite	0.0181	3.2847	0.0265	0.10629	25	0.10608	−15.96	3.35	3.17
	F50-9281	Spinel peridotite	0.0163	6.0853	0.0129	0.10793	21	0.10783	−14.58	3.02	2.94
	L42-13	Olivine megacryst	0.0372	0.0537	3.3356	0.13878	32	0.11283	−10.61	0.19	2.28
	F50-01	Chromite separate	0.4067	1.4007	1.3969	0.11955	28	0.10869	−13.90	future	2.83
	Mid-Ordovician (465 Ma) Mengyin kimberlites										
	SD-9804	Garnet lherzolite	0.0511	2.6152	0.0939	0.11138	16	0.11064	−12.35	3.14	2.57
	SD-9405*	Peridotite	0.2869	2.8790	0.4800	0.12216	12	0.11843	−6.18	future	1.46
	SL-2001	Garnet lherzolite	0.0514	3.1465	0.0785	0.11041	24	0.10980	−13.02	3.16	2.68
	Sv1b-12	Garnet lherzolite	0.0441	1.5192	0.1395	0.11462	20	0.11353	−10.06	2.99	2.19
	Sv1b-11	Spinel peridotite	0.1187	5.2012	0.1097	0.11143	18	0.11057	−12.41	3.28	2.58
	Sv1b-16	Pyroxenite	0.0657	0.1330	2.3745	0.17268	25	0.15421	22.16	1.32	future
	Early Cretaceous (125 Ma) Fangcheng basalts										
	FC6-1-2	Pyroxenite	0.0497	0.0675	3.5402	0.14678	30	0.13200	3.30	–	–
	FC6-2-2	Pyroxenite	0.0498	0.4924	0.4865	0.12162	27	0.11959	−6.42	–	–
	FC25-2	Pyroxenite	0.0414	2.3601	0.0808	0.15871	31	0.15837	23.93	–	–

Values of PUM: $^{187}Os/^{188}Os = 0.1296$ and $^{187}Re/^{188}Os = 0.433$ (Brandon et al. 2001), are used for the calculation of T_{RD} and T_{MA} ages. $\lambda_{Re} = 1.666 \times 10^{-11}year^{-1}$. Emplacement ages of the Paleozoic kimberlites and Mesozoic basalts were used to calculate the initial isotopic ratios. For samples from Ningyuan, the average age of 141 Ma was used

*Data from Gao et al. (2002). Future means the negative age. – means uncalculated since the age for Fangcheng pyroxenites could be meaningless

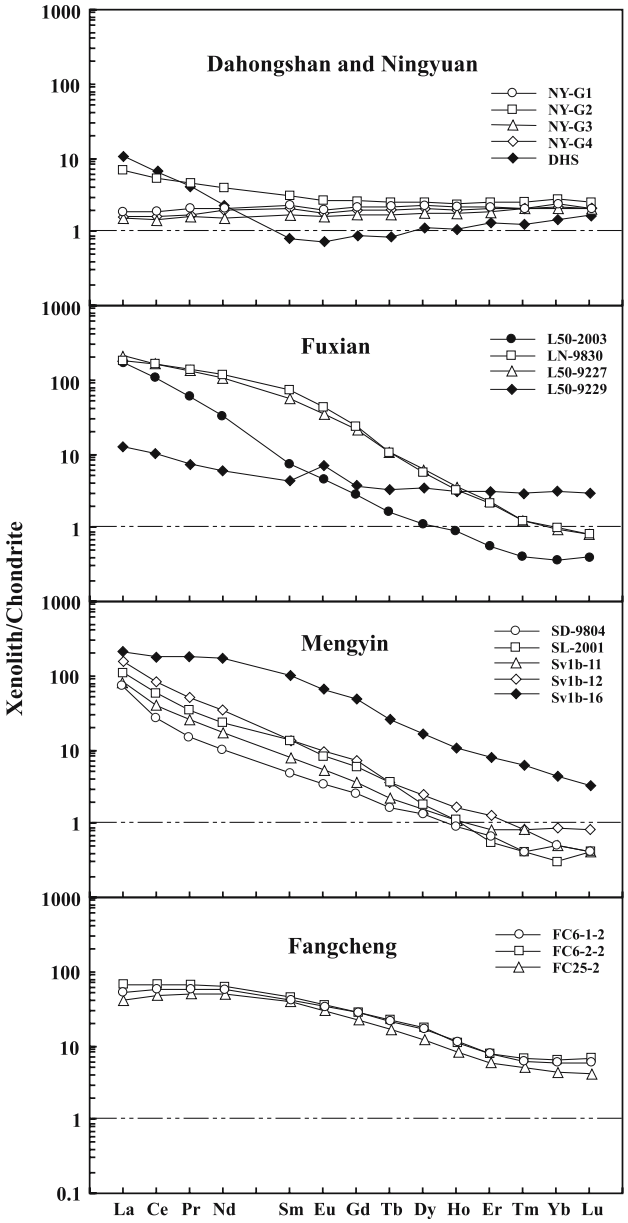

Fig. 2 Chondrite-normalized trace element patterns for the xenoliths from Paleozoic kimberlites and Mesozoic basalts, eastern China. Chondrite values are from Anders and Grevesse (1989)

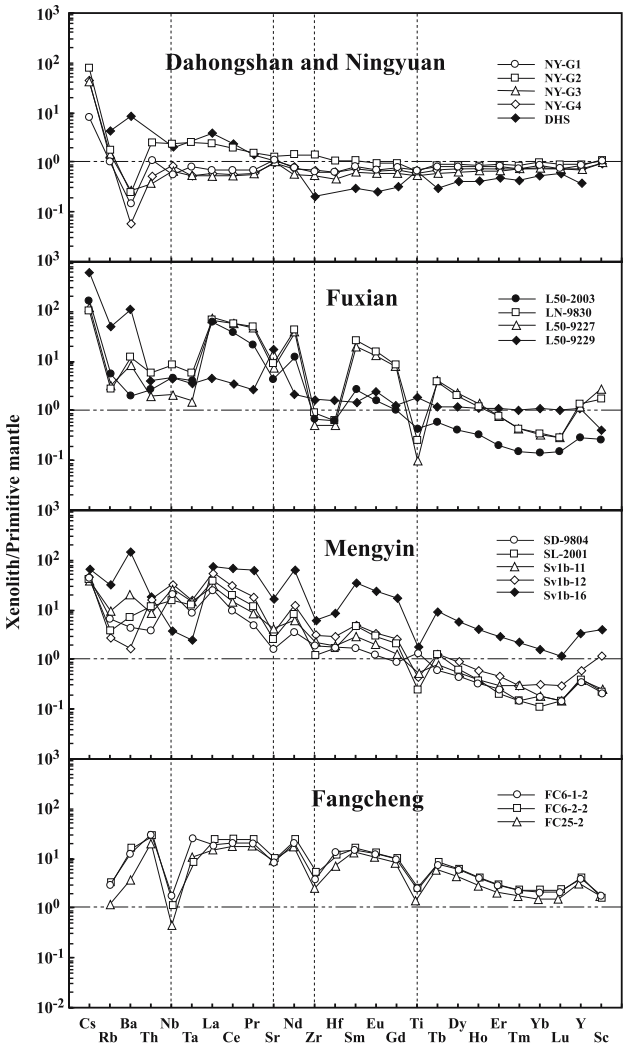

Fig. 3 Primitive mantle-normalized trace element spidergrams for the xenoliths from Paleozoic kimberlites and Mesozoic basalts, eastern China. Primitive mantle values are from McDonough and Sun (1995). Ti concentration is calculated from the TiO_2 content

(typically <1.0; Mitchell and Keays 1981), which is again indicative of a less refractory composition.

Sr and Nd isotopic ratios are slightly more "enriched" than bulk silicate Earth (Table 3 and Fig. 5). Zhang et al. (2001) show that regression of whole rock and cpx, gt, opx mineral separates yields a line in the Rb-Sr isotopic diagram corresponding to 519 Ma. This sample has relatively high Re (0.3 ppb) and Os (4 ppb) (Table 4) close to the primitive mantle values (Fig. 6) and $^{187}Os/^{188}Os$ slightly lower than primitive upper mantle (PUM = 0.1296). It gives a young Re depletion age (T_{RD} = 1.04 Ga), reflecting its high $^{187}Os/^{188}Os$ (~0.1240), and an unrealistic melt depletion age (T_{MA} = 4.7 Ga, older than the age of the Earth), reflecting the high $^{187}Re/^{188}Os$ (~0.36) (Table 4).

Ningyuan spinel lherzolite xenoliths

The Ningyuan spinel lherzolite xenoliths show fertile compositions (Table 2; e.g., CaO = 3.5–4.0%, Al_2O_3 = 3.2~3.6%), similar to PUM (~3.3% and 4.1%, respectively; Hart and Zindler 1986), and Mg#s are also low (88–89). They show nearly flat REE patterns (Fig. 2) with a slightly LREE enrichment in sample NY-G2 and REE concentrations slightly lower than average primitive mantle (Fig. 3). They are enriched in Cs and depleted in Ba, but do not show HFSE anomalies (Fig. 3). Rb and Sr abundances

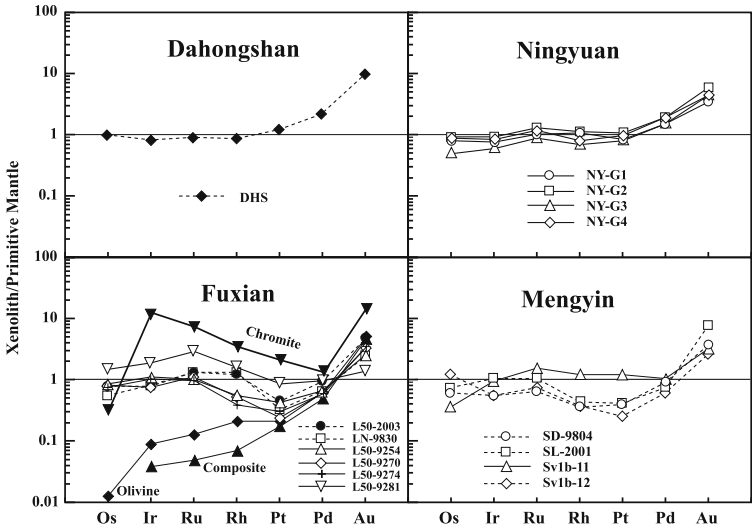

Fig. 4 Primitive mantle-normalized Os, PGE and Au diagrams for the xenoliths and xenocrysts from Paleozoic kimberlites and Mesozoic basalts, eastern China. Primitive mantle values are from Barnes et al. (1988): Os 4.2 ppb, Ir 4.4 ppb, Ru 5.6 ppb, Rh 1.6 ppb, Pt 8.3 ppb, Pd 4.4 ppb, and Au 1.4 ppb. *Solid line* and *dash line* represent the spinel peridotite and garnet peridotite, respectively

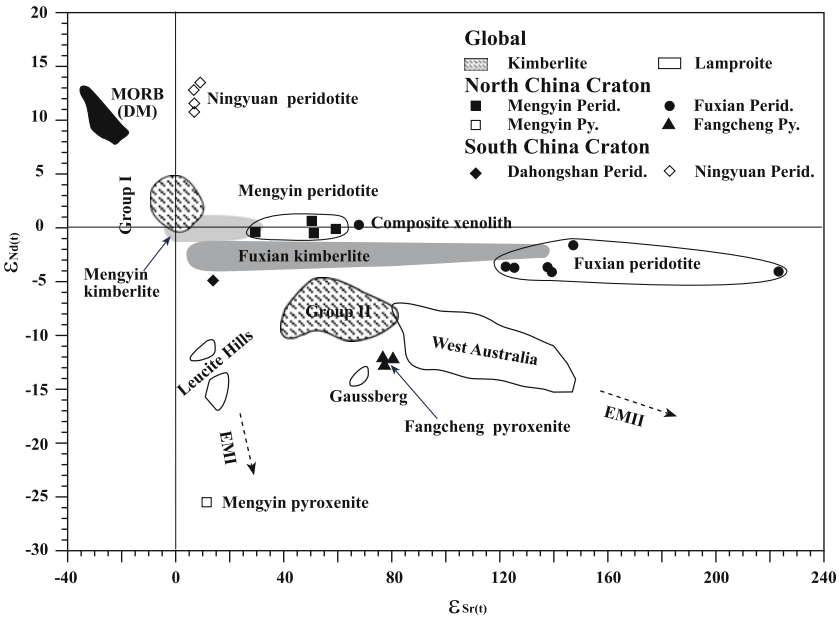

Fig. 5 Sr and Nd isotopic diagram for the xenoliths from Paleozoic kimberlites and Mesozoic basalts, eastern China. εNd(t) and εSr(t) are the deviations from the Chondrite Uniform Reservoir values in parts per 10^4 at the time of eruption. Data of Fuxian and Mengyin kimberlites (Chi and Lu 1996; Tompkins et al. 1999; Zhang and Yang 2007) and global kimberlites and lamproites (Hawkesworth et al. 1990) are plotted for comparison

are close to the value of the primitive mantle, as are PGE and Os concentrations (Barnes et al. 1988) although again Pd is enriched along with Au (Pd/Ir = 2–2.53, Table 2 and Fig. 4).

The Ningyuan xenoliths have high $\varepsilon_{Nd}(t)$ (11–13.5) and Sr isotope ratios slightly higher than bulk Earth ($\varepsilon_{Sr}(t)$ = 6.6–9.2) at the time of basalt eruption (131–151 Ma, Wang (1991); an intermediate value of 141 Ma is used for the correction). Os concentrations (Fig. 6) are close to primitive mantle abundances (2–3.8 ppb; Table 4), but there is a large range in Re abundances (0.12–0.98 ppb). All samples show nearly identical $^{187}Os/^{188}Os$ ratios (Fig. 7b), similar to the Dahongshan garnet lherzolite. Three xenoliths give T_{RD} ages of ~1 Ga like the Danhongshan sample (Table 4; Fig. 7a); one sample gives a younger T_{RD} of ~0.7 Ga. The xenoliths yielded variable T_{MA} ages of 2.3–3.3 Ga. The T_{MA} age of one sample is negative, due to its very high $^{187}Re/^{188}Os$ ratio (~1.2 compared to ~0.3 in the other samples, Table 4).

Fuxian peridotitic xenoliths and xenocrysts

Peridotites

Garnet and spinel peridotites from the Fuxian kimberlite field are strongly serpentinized and carbonatized, except for one relatively fresh sample (L50–2003; Table 2), which is a garnet-bearing peridotite containing kelyphitic pyropes and olivine relicts with Fo as high as 92. The highly

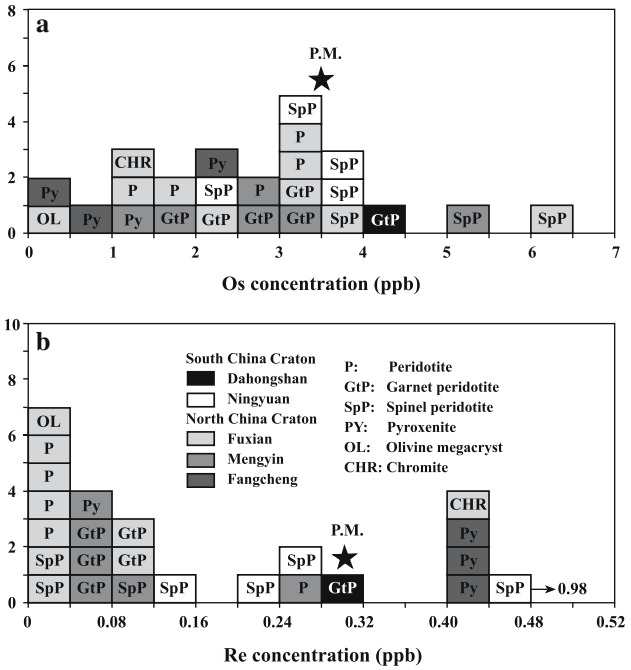

Fig. 6 Histograms of Os (**a**) and Re (**b**) concentrations for the xenoliths from Paleozoic kimberlites and Mesozoic basalts, eastern China. Data for Paleozoic kimberlite-borne xenoliths from Gao et al. (2002) are included. "P.M." denotes primitive mantle values from McDonough and Sun (1995)

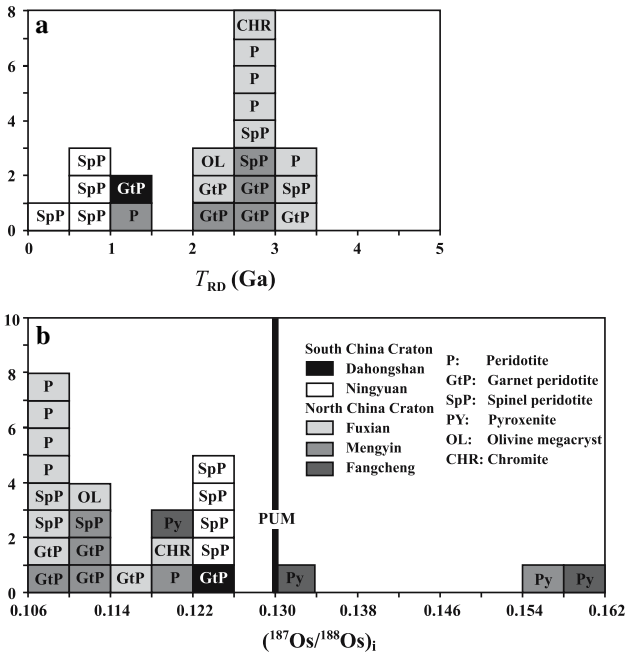

Fig. 7 Histograms of Re-depletion (T_{RD}) model ages in billions of years (**a**) and initial $^{187}Os/^{188}Os$ (**b**) for the xenoliths at the time of host magma eruption. PUM is primitive upper mantle composition of Meisel et al. (2001). Data for Paleozoic kimberlite-borne xenoliths from Gao et al. (2002) are included

serpentinized peridotites have very high REE concentrations and highly fractionated LREE-enriched patterns with HFSE depletions (Figs. 2, 3). The relatively fresh sample L50–2003 also shows LREE-enrichment and extremely high LREE/HREE (La_N/Yb_N = 474), despite lower REE abundances than the highly serpentinized samples (Fig. 2). All the peridotite xenoliths from Fuxian kimberlites display very similar and "sinusoidal" primitive mantle-normalized Os-PGE-Au patterns (Fig. 4), with a positive slope from Os to Ru, a negative slope from Ru to Pt, and a positive slope from Pt to Au. Sample L50–9281 has much higher PGE abundances than the others (Fig. 4), consistent with the presence of sulphides (Table 1).

Fuxian peridotitic xenoliths show $\varepsilon_{Nd}(t)$ slightly lower than the bulk Earth (-1.7 to -4.2) and extremely high initial Sr isotope ratios ($\varepsilon_{Sr}(t)$ = 122–223; Table 3 and Fig. 5), calculated to a kimberlite emplacement age of 465 Ma (Zhang and Yang 2007). The high Sr likely reflects alteration by a fluid with high $^{87}Sr/^{86}Sr$. The observation that the peridotites have the same initial Nd isotopic ratios but much higher initial Sr isotopic ratios than the host kimberlites (Fig. 5) indicates that the alteration was not associated with the kimberlite emplacement but likely occurred in the lithospheric mantle.

The peridotite xenoliths have variable Os (1–6 ppb) and very low Re (0.01–0.12 ppb; Fig. 6), compatible with the Re–Os data of Fuxian peridotite xenoliths of Gao et al. (2002). The garnet lherzolites have slightly higher Re and lower Os than the spinel peridotites (Fig. 6). Nevertheless, all of them have similar $^{187}Re/^{188}Os$ (~0.11) and $^{187}Os/^{188}Os$ ratios (0.106–0.116, γ_{Os} = -9.3 to -16.0; Fig. 7b). They have T_{RD} ages of 2.0–3.2 Ga, similar to the Fuxian chromite separate (Fig. 8a). They also yield very similar T_{MA} ages of 3.0–3.4 Ga (Table 4), slightly older than the T_{RD} ages. On a Re–Os isochron diagram, even if sample LN-9830 is excluded, the peridotite xenoliths form a positive correlation yielding an errorchron of 3.1 ± 1.5 Ga (Fig. 8b). There are no apparent differences between the garnet and spinel peridotites in terms of their Os isotopic compositions and PGE abundances.

Composite xenolith

A composite xenolith (F50–9229) is a spinel lherzolite interlayered with garnet granulite (c.f. Zhang 2006). It has low Mg# (77) and high Al_2O_3 (~17%, vs. 0.7–2.2%) relative to Fuxian peridotite xenoliths (Table 2). It is LREE-enriched and shows a positive Eu anomaly (Fig. 2). It is extremely enriched in some LILE (e.g., Cs = 12.3 ppm, Ba = 717 ppm, Sr = 350 ppm). PGE abundances are extremely low, and IPGE (Os, Ir, Ru) are depleted relative to the PPGE (Rh, Pt, Pd) such that Pd/Ir = 13 (Fig. 4). It

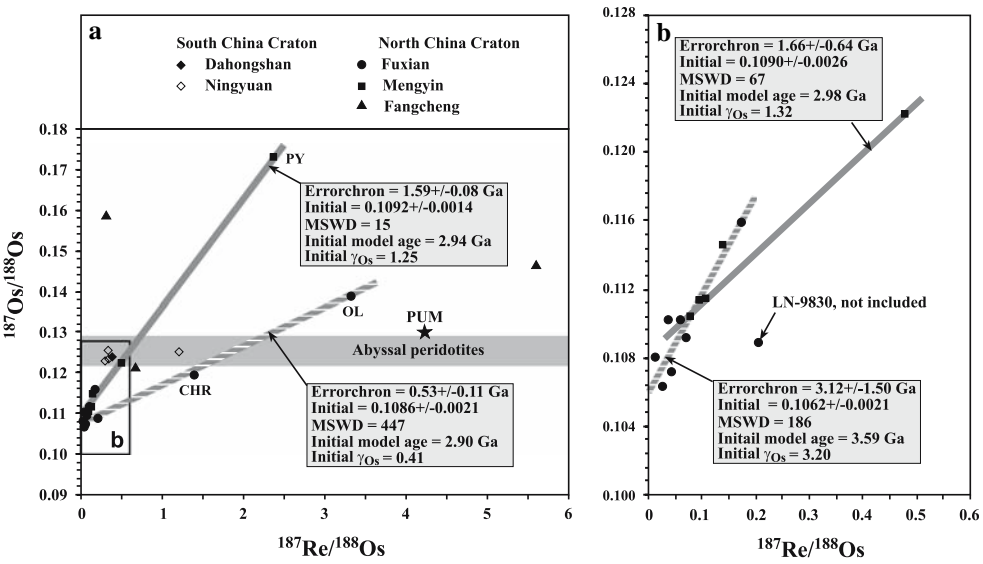

Fig. 8 **a** $^{187}Re/^{188}Os$ versus $^{187}Os/^{188}Os$ for the xenoliths from Paleozoic kimberlites and Mesozoic basalts with the Re–Os errorchrons for the xenoliths from Fuxian and Mengyin Paleozoic kimberlites. **b** A magnification of the rectangle area in **a**. PUM is primitive upper mantle composition of Meisel et al. (2001). *Shaded field* represents range of $^{187}Os/^{188}Os$ in abyssal peridotites (Brandon et al. 2001 and references therein). Data for Paleozoic kimberlite-borne xenoliths from Gao et al. (2002) are included. Data regressed and MSWD determined using Isoplot program of Ludwig (2003)

has slightly higher Nd and much lower Sr isotope ratios than Fuxian peridotites (Fig. 5). The presence of garnet granulite rather than eclogite likely reflects the conditions of the cratonic geotherm beneath the Fuxian region of the North China Craton during the Paleozoic.

Olivine megacryst

An elliptoid and egg-sized olivine xenocryst (L42–13) is highly serpentinized. The olivine has very low PGE contents and IPGE are depleted relative to PPGE (Pd/Ir = 7.15, Fig. 4). It has extremely low Re and Os concentrations (0.04 and 0.05 ppb, respectively, Table 4 and Fig. 6), but high $^{187}Re/^{188}Os$ compared with the peridotites (>3 vs. <0.21), as well as high $^{187}Os/^{188}Os$ ($\sim$0.14 vs. $\sim$0.11).

Chromite separate

Chromite separate F50–01 has very high PGE contents (for instance, Ir = 52.2 ppb, more than an order of magnitude higher than the next enriched Fuxian sample) and enrichment of IPGE relative to the PPGE (Pd/Ir = 0.11), but also low Os and high Au (Fig. 4). The Re and Os abundances and $^{187}Os/^{188}Os$ are generally consistent with those reported by Wu et al. (2006) for chromite separates from the same kimberlite field. The fact that chromites separated from the Fuxian kimberlites have generally higher Re and lower Os than typically found in chromites from ophiolites (Walker et al. 2002) indicates that these might be disaggregated from the lithospheric mantle peridotites, and thus represent the litospheric mantle. If true, then chromite Os isotopic data can be used to constrain the age of the lithospheric mantle. The chromite separate studied here yields a T_{RD} age of 2.83 Ga and falls right in the middle of ages for the North China Craton (Table 4, Fig. 7a). If this chromite separate and the olivine xenocryst plotted in a Re–Os isochron diagram with the peridotites, all the Fuxian data form an errorchron of 0.53 ± 0.11 Ga with an initial $^{187}Os/^{188}Os$ ratio of 0.1086 (Fig. 8a). Although we do not put any emphasis on any implications of this age, we note that the initial Os isotopic ratio gives a PUM model age of 2.9 Ga, similar to the T_{RD} ages given by the chromite separate as well as the peridotites.

Mengyin peridotitic and pyroxenite xenoliths

Peridotites

Garnet (SD-9804, SL-2001, Sv1b-12) and spinel (Sv1b-11) peridotites from the Mengyin kimberlite field are highly serpentinized, but not as strongly as those from the Fuxian kimberlite field, as shown by lower loss on ignition (13–14%). Unlike the Fuxian peridotites, those from Mengyin are not strongly carbonatized, as indicated by low CaO (<1.2%; Table 2). They have high REE abundances and highly fractionated LREE-enriched patterns (La_N/Yb_N = 150–369; Fig. 2). Also unlike the Fuxian xenoliths, they are slightly depleted in HFSE such as Ti, Zr, Hf, Ta (Fig. 3). The three garnet peridotitic xenoliths from the Mengyin kimberlites display similar U-shaped primitive mantle-normalized Os-PGE-Au patterns (Fig. 4), with a negative slope from Os to Pt and a positive slope from Pt to Au. The spinel peridotitic xenolith shows a sinusoidal pattern, similar to the Fuxian peridotites. The PGE concentrations are similar to those in Fuxian peridotites.

Like the Fuxian peridotites, the Mengyin peridotites show a small range of $\varepsilon_{Nd}(t)$ (−0.6 to 0.6), in this case close to bulk Earth values. The three garnet peridotites have higher Sr isotope ratios ($\varepsilon_{Sr}(t)$ = 50–60) than the spinel peridotite ($\varepsilon_{Sr}(t)$ = 30), calculated to a kimberlite emplacement age of 465 Ma (Table 3, Fig. 5).

The Mengyin peridotite xenoliths have variable Os (1.5–5.2 ppb) concentrations, similar to Fuxian peridotites (Table 4, Fig. 6). However, Mengyin peridotites have slightly higher Re (0.05–0.28 ppb). The three garnet peridotites have much lower Re (<0.06 ppb) than the spinel peridotite (>0.11 ppb, Table 4, Fig. 6), a distinction not seen in the Fuxian garnet and spinel peridotites. All the Mengyin peridotite xenoliths possess nearly identical initial $^{187}Os/^{188}Os$ (0.110–0.115, γ_{Os} = −10 to −12.4), and give similar T_{RD} ages of 2.2–2.7 Ga, typical of North China Craton xenoliths, but with a slightly lower average value than the Fuxian peridotites. These initial $^{187}Os/^{188}Os$ values are lower than the Mengyin sample analyzed by Gao et al. (2002) (∼0.118, SD-9405, listed in Table 4), which also gives a younger T_{RD} age (∼1.5 Ga) and a future T_{MA} age. Peridotites from both the Mengyin and Fuxian kimberlites have similar T_{MA} ages, averaging ∼3.0 Ga. The Mengyin peridotitic xenoliths form an errorchron on a Re–Os isochron diagram with an age of 1.66 ± 0.64 Ga (Fig. 8b). Though its meaning is unclear, the initial Os ratio gives a model age of 2.98 Ga, consistent with the T_{MA} ages. Although the Mengyin garnet and spinel peridotites show differences in PGE and Re, Os contents, the Os isotopic compositions and model ages do not show apparent differences.

Pyroxenite

A macrocrystic pyroxenite xenolith (Sv1b-16) from the Mengyin kimberlite has low MgO (14 vs. >20%) and is more enriched in Al_2O_3, CaO and K_2O (Table 2) than pyroxenite xenoliths from Mesozoic Fangcheng basalts, reflecting its mineral assemblage with some amphibole and plagioclase. It is LREE-enriched (La_N/Yb_N ∼47.6) and has very high REE but has low HFSE and Sr (Figs. 2, 3). While Nb and Ta are lower than the peridotites, Sr is higher.

The pyroxenite shows "EM1-like" Sr-Nd isotopes (Fig. 5), that is, a very low Nd isotope ratio ($\varepsilon_{Nd}(t)$ = −26) and at the same time low initial $^{87}Sr/^{86}Sr$ ($\varepsilon_{Sr}(t)$ ∼11.3). It has low Os (0.133 ppb) and extremely high $^{187}Re/^{188}Os$ (2.4). Nevertheless, it has a high initial $^{187}Os/^{188}Os$ (0.154, γ_{Os} = 22, Fig. 7b), thus is completely different from the Re–Os isotopes of the peridotites (Table 4). It has a future T_{RD} age and a T_{MA} age of 1.32 Ga. It should be noted that this T_{MA} age overlaps the Re–Os errorchron age of the Mengyin peridotites, perhaps indicating that this pyroxenite is a sample of the melts that caused metasomatism of the lithospheric peridotites.

Fangcheng pyroxenite xenoliths

As noted above, the pyroxenite xenoliths from the Fangcheng basalts have higher MgO and lower CaO and Al_2O_3 then the Mengyin pyroxenite (Table 2). They also have similarly LREE-enriched patterns, and low HFSE and LILE (Table 2 and Figs. 2, 3).

The Fangcheng pyroxenites have enriched initial Sr-Nd isotope ratios, corrected to 125 Ma ($\varepsilon_{Sr}(t)$ = 76–81 and $\varepsilon_{Nd}(t)$ ∼ −12; Fig. 5). These Sr-Nd isotopic ratios are very similar to the host basalts ($\varepsilon_{Sr}(t)$ = 75 to 82; $\varepsilon_{Nd}(t)$ = −12.8 to −14.4; Zhang et al. 2002). These pyroxenites show extremely large variations in Os abundances (0.06–2.36 ppb), $^{187}Re/^{188}Os$ (0.08 ∼ 3.54) and initial $^{187}Os/^{188}Os$ (0.12–0.16) (Table 4; Figs. 6, 7, 8) though the Re abundances are relatively constant, leading to exceedingly large γ_{Os} (−6.4 to 24). The currently available Fangcheng Re–Os data are not as systematic as the other localities, and less easy to interpret, and therefore are not used in the following discussion.

Discussion

Ancient SCLM during the Paleozoic beneath the eastern North China Craton

The Re–Os data for garnet and spinel peridotitic xenoliths from the Fuxian and Mengyin diamondiferous kimberlites document the presence of Archean lithospheric mantle beneath the eastern North China Craton during Ordovician time. Two Fuxian xenoliths in the pioneering work of Gao et al. (2002) are clearly Archean, with T_{RD} and T_{MA} ages greater than 2.5 Ga, suggesting that the SCLM beneath the Fuxian region was formed in the Archean. Their conclusion is further confirmed by this study on additional peridotitic xenoliths from the same kimberlite field, which dominantly give T_{RD} ages of 2.7–3.2 Ga and the T_{MA} ages of 2.9–3.4 Ga except for one sample (L50–2003 for the T_{RD} age and LN-9830 for the T_{MA} age; Table 4, Fig. 7a). A chromite separate from the Fuxian kimberlites also gives an Archean T_{RD} age of ∼2.8 Ga (Table 4). The low Re in these xenoliths may be a primary feature and suggests that intensive serpentinization did little to increase the Re/Os ratio or alter $^{187}Os/^{188}Os$ of peridotitic xenoliths. The peridotite xenoliths from the Mengyin kimberlites analyzed in this study all yield effectively the same T_{RD} ages of ∼2.6 Ga and T_{MA} ages of 3.0–3.3 Ga (Table 4; Fig. 7a). This is consistent with an Archean T_{RD} age of 2.69 Ga of a

chromite separate from Mengyin kimberlites by Wu et al. (2006). However, a Mengyin peridotite analysed by Gao et al. (2002) has significantly higher Re/Os and $^{187}Os/^{188}Os$ and a younger T_{RD} age of ~1.5 Ga. This sample also has a negative T_{MA} age, indicating that it experienced Re addition after the original melt depletion event. If we assume that melt depletion occurred in the Archean (based on our data), then the Proterozoic Re depletion age may indicate Re addition during the Proterozoic, perhaps at around 1.5 Ga. This is consistent with the Proterozoic melt depletion age of the pyroxenite xenolith from the Mengyin kimberlite (T_{MA} age = 1.32 Ga, Table 4). Ages of ~1.4 Ga can also be found in peridotites from the Dabie-Sulu orogen (Zheng et al. 2006a, d). The 1.6 Ga Re–Os errorchron for the Mengyin peridotites (Fig. 8) also supports the idea that something important happened to these rocks in the mid-Proterozoic. In addition, the SCLM beneath the northern margin of the eastern North China Craton might have slightly younger ages as the mantle peridotitic xenoliths from the Tieling kimberlites give the T_{RD} ages of Paleoproterozoic (1.8–2.3 Ga) (Wu et al. 2006).

Overall, the Re–Os data demonstrate that SCLM beneath the central part of the eastern North China Craton had Archean and Paleoproterozoic ages during the Paleozoic. Moreover this is the case for both shallow and the deeper lithospheric mantle, as the ancient ages are observed in both garnet and spinel facies xenoliths. However, this Archean lithospheric mantle was later modified by melts. The best evidence for melt modification of the Archean lithosphere comes from the overlapping mid-Proterozoic Re–Os errorchron of the Mengyin peridotites and the 1.32 Ga T_{MA} age of the Mengyin pyroxenite (Fig. 8).

Compositional stratification in the SCLM before lithospheric thinning?

Compositional distinctions of mantle peridotite xenoliths sampled by the Paleozoic kimberlites, (such as forsterite compositions of olivines) compared with those in the Cenozoic basalts, have raised the question of whether the SCLM beneath the eastern North China Craton was compositionally stratified before it was thinned. For example, one might argue that the highly refractory garnet peridotitie xenoliths sampled by the Paleozoic kimberlites (Fo > 92; Zheng et al. 2006b) were derived from deeper mantle that was completely lost during lithosphere thinning. That is, the relatively fertile spinel peridotite xenoliths from the widespread Cenozoic basalts of the North China Craton (generally Fo $\leq$ 92; Fan et al. 2000; Rudnick et al. 2004) are from shallower mantle that may be compositionally different from the deeper garnet-facies mantle. The few spinel-bearing peridotitic xenoliths entrained in Paleozoic kimberlites have high Fo contents in olivines similar to those from the garnet peridotitic xenoliths (Zheng et al. 2006b), suggesting that there were no obvious compositional differences between the garnet- and spinel-facies SCLM before the lithospheric thinning. This conclusion is supported by the PGEs and Re–Os isotopic systematics of the garnet and spinel peridotite xenoliths in this study.

Both the garnet and spinel peridotitic xenoliths from the Fuxian kimberlites display similar primitive mantle-normalized Os-PGE-Au patterns (Fig. 4). They have very similar initial $^{187}Os/^{188}Os$ (0.106–0.116, Table 4; Fig. 7b), although the garnet lherzolites have slightly higher Re and lower Os than the spinel peridotites (Table 4; Fig. 6). All these peridotite xenoliths give similar (Archean) T_{RD} ages of 2.7–3.2 Ga and T_{MA} ages of 3.0–3.4 Ga (Table 4; Fig. 7a). Thus, there are no apparent differences in Os isotopes or PGE concentrations between the garnet and spinel peridotites in the Fuxian locality.

From Mengyin, three garnet peridotitic xenoliths display similar U-shaped primitive mantle-normalized Os-PGE-Au patterns (Fig. 4), slightly different from the sinusoidal pattern for a spinel peridotite. The spinel peridotite shows lower $\varepsilon_{Sr}(t)$ than the garnet peridotites (Fig. 5). The slight differences may be produced by Proterozoic metasomatism in the garnet-facies lithospheric mantle. More significant is that all the garnet and spinel peridotites show effectively the same initial $^{187}Os/^{188}Os$ and the similar (Archean) T_{RD} (~2.7 Ga) and T_{MA} (3.0–3.3 Ga) ages (Table 4; Fig. 7a).

We conclude that apparent compositional stratification of the SCLM before its thinning is not favored by the Fo numbers, PGEs and Re–Os isotopic data. This is also the case for the SCLM beneath the Archean Kaapvaal Craton (Pearson et al. 1995, 1999).

Mechanisms for lithosphere thinning and its transformation

Re–Os isotopic data of mantle xenoliths can be used to test models of lithospheric thinning. Our data indicate that the lithospheric mantle of the North China Craton had ages as old as Archean prior to kimberlite emplacement during the Paleozoic, and lacked compositional stratification in garnet and spinel facies mantle. The delamination model of Wu et al. (2003) and Gao et al. (2004) suggests that the present-day lithospheric mantle should have young Phanerozoic ages, since it must be newly accreted since the thinning. On the other hand, the thermo-mechanical erosion model of Xu (2001) implies an Archean age for the remaining lithospheric mantle. Compositional transformation through peridotite-melt reaction as suggested by Zhang (2005)

implies a lithospheric mantle with ages from Archean to Phanerozoic, as this process could reset the ages of parts of the lithosphere.

Re–Os data have been published for Cenozoic basalt-hosted peridotitic xenoliths from different localities of the North China Craton (Fig. 1). In the central zone, peridotite xenoliths from Hannuoba give a Paleoproterozoic Re–Os isochron age of 1.91 ± 0.22 Ga (Gao et al. 2002), while the crustal age is Archean. Mantle xenoliths from Fanshi, about 200 km to the south give Archean T_{RD} ages (Rudnick et al. 2006). These data are consistent with the suggestion by Gao et al. (2002) that the lithosphere beneath Hannuoba formed in the Archean, but was replaced in the Paleoproterozoic. In the eastern North China Craton, peridotite xenoliths from Qixia give predominantly Phanerozoic T_{RD} ages (0.22–0.75 Ga), although the sample having the highest Fo in olivine and Cr# in spinel gives an older age (T_{RD} = 1.32 Ga; Gao et al. 2002) (Fig. 9), and those from Kuandian show a large T_{RD} age range from Paleoproterozoic to Tertiary (T_{RD} = 0.3–2.18 Ga; Wu et al. 2006) (Fig. 9). Although $^{187}Os/^{188}Os$ ratios do not correlate with melt depletion or fertility indicators such as Al_2O_3 in the Kuandian xenoliths, the two peridotites with the highest Fo in olivines and Cr# in spinels give the oldest T_{RD} ages (Wu et al. 2006), implying that older Re–Os ages may generally correlate with the Fo contents in olivines. On the northern and southern margins of the North China Craton at Lonngang and Nushan, respectively, Re–Os ages in mantle xenoliths are Proterozoic to Phanerozoic (Wu et al. 2003; Zhi and Qin 2004) (Fig. 9).

These studies show that the present-day lithospheric mantle beneath the North China Craton has a mixture of ages, from Archean or Paleoproterozoic to Phanerozoic (Fig. 9). Therefore, we can conclude that the Archean (and Proterozoic) mantle peridotitic xenoliths represent the remnants of thinned Archean lithospheric mantle, and the Phanerozoic ones represent the lithospheric mantle that is newly accreted after the thinning, or formed through interaction with the massive addition of melts during the Mesozoic (and Cenozoic). The latter case would imply that melt addition transformed highly refractory peridotites to fertile ones, and also introduced Re into peridotites, which would lower the Re–Os isotopic ages. Evidence for melt circulation in the lithospheric mantle and interaction with peridotites has been identified in xenocrysts and pyroxenite xenoliths from the Mesozoic Fangcheng basalts (Zhang et al. 2007) as well as in composite xenoliths from the Cenozoic Hannuoba basalts (Liu et al. 2005). The pyroxenite xenoliths in this study (Table 4) show variable $^{187}Re/^{188}Os$ and high $^{187}Os/^{188}Os$ ratios, and these characteristics could be the products of the melt circulation. The evidence suggests that melt infiltration plays an important role in the transformation of the lithospheric mantle.

Our conclusion that the Archean refractory lithospheric mantle had been partially refertilized to Phanerozoic fertile lithospheric mantle is also supported by the variable mineral compositions, such as Fo 93–83 values in olivines, found to be widespread in mantle peridotite xenoliths and xenocrysts from Mesozoic and Cenozoic basalts of the North China Cration (Song and Frey 1989; Fan et al. 2000; Zheng et al. 1998, 2001; Yan et al. 2003; Rudnick et al. 2004; Zhang 2005; Tang et al. 2004; Ying et al. 2006; Wu et al. 2006). The xenoliths with Archean T_{RD} ages from the Mengyin and Fuxian kimberlites still have olivine relicts with Fo as high as 92–94. However, a compilation of published data (Zhang et al. 2006) shows that such high Fo in olivines is rare in mantle peridotitic xenoliths or xenocrysts from Mesozoic and Cenozoic basalts on the North China Craton, except for the Hebi (Zheng et al. 2001). This also implies that ancient refractory lithospheric mantle was transformed to young fertile mantle through multiple

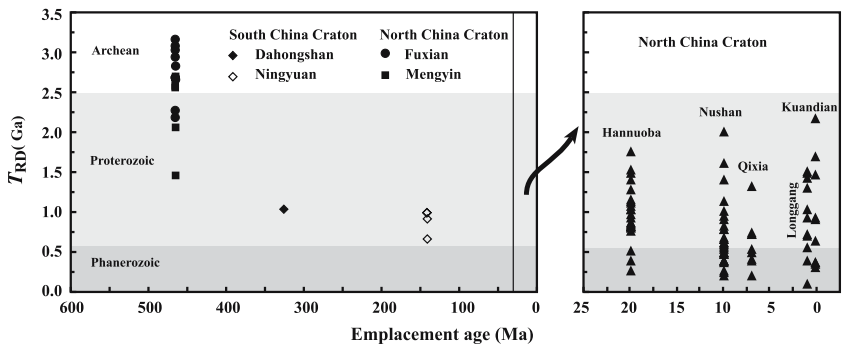

Fig. 9 Emplacement age (Ma) of host magma versus Re depletion age (Ga) of mantle xenoliths from Paleozoic kimberlites and Mesozoic and Cenozoic basalts from the North China and South China Cratons. Re–Os data of mantle xenoliths from the Cenozoic basalts on the North China Craton are collected from Zhi et al. (2001), Gao et al. (2002), Wu et al. (2003, 2006), Xia et al. (2004), Zhi and Qin (2004). All the T_{RD} ages were re-calculated from the original data relative to the value of PUM: $^{187}Os/^{188}Os$ = 0.1296 and $^{187}Re/^{188}Os$ = 0.433 (Brandon et al. 2001)

events of peridotite-melt interaction. This could be the result of decompressional melting during upwelling of asthenosphere in association with lithospheric thinning.

Neoproterozoic Re–Os isotopic resetting of the Yangtze Block

The South China Craton, like the North China Craton, has Archean crust, particularly in the Yangtze Block. Recent work on zircon U-Pb ages and Hf isotopes of gneiss xenoliths from early Carboniferous lamproite/kimberlite diatremes suggest the widespread presence of Archean basement with zircon ages of 2.5–2.6 and 2.8–2.9 Ga and Hf model ages of 2.6 to 3.5 Ga (Zheng et al. 2006c). This implies that the lithospheric mantle beneath the craton originally formed in the Archean. However, the only garnet peridotitic xenolith analyzed from the Yangtze Block (from Dahongshan, Fig. 1) gives a much younger Neoproterozoic T_{RD} age of 1.04 Ga (Table 4). The xenolith has relatively high Re (0.3 ppb) and Os (4 ppb), close to primitive mantle values (Fig. 6). Its initial $^{187}Os/^{188}Os$, slightly lower than PUM (Fig. 7b), falls in the range of global abyssal peridotites (Brandon et al. 2001). Interestingly, spinel peridotite xenoliths from the Mesozoic Ningyuan basalts have very similar Os (2–3.8 ppb) concentrations and initial $^{187}Os/^{188}Os$ ratios (Table 4) to the Dahongshan garnet lherzolite, despite a large range of Re concentrations (0.12–0.98 ppb) and $^{187}Re/^{188}Os$ (0.3–1.2). Three of the Ningyuan xenoliths also show very similar Neoproterozoic T_{RD} ages of $\sim$1 Ga and variable T_{MA} ages of 2.3–3.3 Ga (Table 4). This may indicate that the Archean lithospheric mantle beneath the South China Craton has undergone considerable Re–Os isotopic resetting since its formation, perhaps during the Neoproterozoic amalgamation of the Cathaysia Block in the south and the Qinling-Dabie belt in the north. It has been suggested that extensive Neoproterozoic magmatism along the southeastern margin of the Yangtze Block was associated with the Jiangnan island arc, and the adjacent ocean existed as early as $\sim$1.0 Ga (Zhou et al. 2002 and references therein). The mafic protolith for the Dabie eclogites, with positive $\varepsilon_{Hf}(t)$ values, give depleted mantle Hf model ages of $\sim$0.8 Ga (Zheng et al. 2006e). These Hf model ages are similar to ages for bimodal magmatism in the periphery of the Yangtze Block, and indicate new addition of juvenile continental crust in the region at that time (Li et al. 2003; Zheng et al. 2006c, e).

Lithospheric reworking is also indicated by the petrological and geochemical characteristics of the Dahongshan xenolith (Zhang et al. 2001). Its high Al_2O_3 and CaO contents, compared with global kimberlite-borne garnet lherzolites from Archean cratons (McDonough 1990), indicate a fertile mantle source. The V-shaped REE pattern (Fig. 2) is also considerably different from the general LREE-enriched patterns for garnet peridotite xenoliths of global Archean cratons (McDonough 1990). The PGE concentrations similar to primitive mantle (Fig. 4) are also indicative of less depletion. The enrichments in the PPGE and Re over the IPGE for the Dahongshan and Ningyuan peridotites provide additional evidence for the refertilization of the lithosphere through the mantle metasomatism (Fig. 4). Together, these observations suggest that lithospheric mantle refertilization resulted in considerable resetting of the PGE features and Re–Os isotopic systems.

Conclusions

We draw the following primary conclusions from this study.

(1) Re–Os isotopes in garnet and spinel peridotite xenoliths hosted by the Mengyin and Fuxian diamondiferous kimberlites, emplaced during the early Paleozoic in the North China Craton, further confirm that SCLM of Archean age existed beneath the North China Craton during the Paleozoic.

(2) Comparison of spinel and garnet facies peridotite xenoliths indicates an absence of compositional stratification in the Paleozoic lithospheric mantle.

(3) The Re–Os isotopic features of mantle xenoliths from the Paleozoic kimberlites of the North China Craton are different from peridotitic and pyroxenite xenoliths from Cenozoic and Mesozoic basalts, which show younger Re–Os model ages. The present-day lithospheric mantle beneath this craton has both ancient and recent Re–Os ages.

(4) In the South China Craton, there is a decoupling of ages between the crust and the underlying SCLM in the Yangtze Block, with mantle xenoliths emplaced during the Paleozoic and Mesozoic showing Neoproterozoic T_{RD} ages, suggesting Neoproterozoic resetting of the SCLM beneath the Yangtze Block.

(5) The large range of Re–Os isotopic ages in Phanerozoic xenoliths indicate that lithospheric transformation through melt-peridotite interaction could be a more important mechanism for compositional changes during the Phanerozoic than delamination or thermo-mechanical erosion.

Acknowledgments The authors thank Weiming Fan for providing the Ningyuan samples. We are also indebted to Meifu Zhou and Xiao Fu for their assistance with XRF and ICPMS analyses for major oxides, trace elements and PGE concentrations at the University of Hong Kong, Bernhard Peucker-Ehrenbrink for advice on sparging, which helped greatly in setting up the measurement procedures for Os

isotopes at Lamont, and Alberto Saal for assistance with preparation of Re–Os for analyses. Constructive reviews and comments of T. Grove, R. Carlson, and an anonymous reviewer greatly helped to improve the manuscript. This research was financially supported by funding from the Lamont-Doherty Earth Observatory, as grants from the Nature Science Foundation of China (40534022) and the Knowledge Innovation Program of the Chinese Academy of Sciences (KZCX2-YW-103) to HF Zhang, and a Hong Kong RGC Grant to M Sun. This is LDEO contribution #7063.

References

Anders E, Grevesse N (1989) Abundances of the elements: meteoritic and solar. Geochim Cosmochim Acta 53:197–214

Barnes SJ, Boyd R, Korneliussen A, Nilsson LP, Often M, Pederson RB, Robins B (1988) The use of mantle normalization and metal ratios in discriminating between the effects of partial melting, crystal fractionation and sulfide segregation on platinum-group elements, gold, nickel and copper: examples from Norway. In: Prichard HM, Potts PJ, Bowles JFW, Cribb SJ (eds) Geoplatinum, vol 87. Elsevier, Amsterdam, pp 113–143

Boyd FR (1989) Compositional distinction between oceanic and cratonic lithosphere. Earth Planet Sci Lett 96:15–26

Boyd FR, Gurney JJ, Richardson SH (1985) Evidence for a 150–200 km thick Archaean lithosphere from diamond inclusion thermobarometry. Nature 315:387–389

Boyd FR, Pokhilenko NP, Pearson DG, Mertzman SA, Sobolev NV, Finger LW (1997) Composition of the Siberian cratonic mantle: evidence from Udachnaya peridotite xenoliths. Contrib Mineral Petrol 128:228–246

Brandon AD, Snow JE, Walker RJ, Morgan JW, Mock TD (2001) ^{190}Pt-^{186}Os and ^{187}Re-^{187}Os systematics of abyssal peridotites. Earth Planet Sci Lett 177:319–335

Chen JF, Jahn BM (1998) Crustal evolution of southeastern China: Nd and Sr isotopic evidence. Tectonophysics 284:101–133

Chen JF, Foland KA, Xing FM, Xu X, Zhou TX (1991) Magmatism along the southeast margin of the Yangtze block: precambrian collision of the Yangtze and Cathaysia blocks of China. Geology 19:815–818

Chen L, Zheng TY, Xu WW (2006) A thinned lithospheric image of the Tanlu Fault Zone, eastern China: constructed from wave equation based receiver function migration. J Geophys Res 111:B09312 doi: 10.1029/2005JB003974

Chi JS, Lu FX (1996) The study of formation conditions of primary diamond deposits in China. China University of Geosciences, Beijing, pp 144 (in Chinese)

Deng JF, Mo XX, Zhao HL, Luo ZH, Du YS (1994) Root of the lithosphere underneath eastern China: unrooting and continental remobilization. Mod Geol 8(3):349–356 (in Chinese)

Deng JF, Mo XX, Zhao HL, Wu ZX, Luo ZH, Su SG (2004) A new model for the dynamic evolution of Chinese lithosphere: continental roots-plume tectonics. Earth Sci Rev 65:223–275

Dobbs PN, Duncan DJ, Hu S, Shee SR, Colgan E, Brown MA, Smith CB, Allsopp HL (1994) The geology of the Mengyin kimberlites, Shandong, China. In: Meyer HOA, Leonardos OH (eds) In: Proceedings 5th Int Kimb Conf 1. Diamonds: characterization, genesis and exploration. CPRM, Brasilia, pp 106–115

Fan WM, Menzies MA (1992) Destruction of aged lower lithosphere and accretion of asthenosphere mantle beneath eastern China. Geotectonica et Metallogenia 16:171–180

Fan WM, Zhang HF, Baker J, Jarvis KE, Mason PRD, Menzies MA (2000) On and off the North China Craton: where is the Archaean keel? J Petrol 41:933–950

Fan WM, Guo F, Wang YJ, Zhang M (2004) Late Mesozoic volcanism in the northern Huaiyang tectono-magmatic belt, central China: partial melts from a lithospheric mantle with subducted continental crust relicts beneath the Dabie orogen. Chem Geol 209:27–48

Gao S, Rudnick R, Carlson RW, McDonough WF, Liu YS (2002) Re–Os evidence for replacement of ancient mantle lithosphere beneath the North China craton. Earth Planet Sci Lett 198:307–322

Gao S, Rudnick RL, Yuan HL, Liu XM, Liu YS, Xu WL, Ling WL, Ayers J, Wang XC, Wang QH (2004) Recycling lower continental crust in the North China craton. Nature 432:892–897

Griffin WL, O'Reilly SY, Ryan CG (1992) Composition and thermal structure of the lithosphere beneath South Africa, Siberia and China: proton microprobe studies. International Symposium on Cenozoic Volcanic Rocks and Deep-seated Xenoliths of China and its Environs, Beijing, pp 1–20

Griffin WL, Zhang AD, O'Reilly SY, Ryan CG (1998) Phanerozoic evolution of the lithosphere beneath the Sino-Korean Craton. In: Flower M, Chung SL, Lo CH, Lee TY (eds) Mantle dynamics and plate interactions in East Asia. American Geophysical Union, Washington DC, pp 107–126

Hart SR, Zindler A (1986) In search of a bulk-Earth composition. Chem Geol 57:247–267

Hassler DR, Peucker-Ehrenbrink B, Ravizza GE (2000) Rapid determination of Os isotopic composition by OsO_4 into a magnetic-sector ICP-MS. Chem Geol 166:1–14

Hawkesworth CJ, Kempton PD, Rogers NW, Ellam RM, Van Calsteren PW (1990) Continental mantle lithosphere, and shallow level enrichment processes in the Earth's mantle. Earth Planet Sci Lett 96:256–268

Hu SB, He LJ, Wang JY (2000) Heat flow in the continental area of China: a new data set. Earth Planet Sci Lett 179:407–419

Jordan TH (1975) The continental tectosphere. Rev Geophys Space Phys 13:1–12

Jordan TH (1988) Structure and formation of the continental lithosphere. In: Menzies MA, Cox K (eds) Oceanic and Continental Lithosphere: similarities and differences. J Petrol Special Lithosphere Issue:11–37

King SD (2005) Archean cratons and mantle dynamics. Earth Planet Sci Lett 234:1–14

Kröner A, Composton W, Zhang GW, Guo AL, Todt W (1988) Ages and tectonic setting of Late Archean greenstone-gneiss terrain in Henan Province, China as revealed by single-grain zircon dating. Geology 16:211–215

Li XH, Tatsumoto M, Gui XT (1989) Discovery of the Archean relict zircon (2.5 Ga in age) in Tanghu granite, south China and its significance. Chinese Sci Bull34:206–209 (in Chinese)

Li XH, Zhao JX, McCulloch MT, Zhou GQ, Xing FM (1997) Geochemical and Sm-Nd isotopic study of Neoproterozoic ophiolites from southeastern China: petrogenesis and tectonic implications. Precamb Res 81:129–144

Li ZX, Li XH, Kinny PD, Wang J (1999) The breakup of Rodinia: did it start with a mantle plume beneath South China? Earth Planet Sci Lett 173:171–181

Li XH, Sun M, Wei GJ, Liu Y, Lee CY, Malpas J (2000) Geochemical and Sm-Nd isotopic study of amphibolites in the Cathaysia Block, southeastern China: evidence for an extremely depleted mantle in the Paleoproterozoic. Precamb Res 102:251–262

Li JH, Hou GT, Huang XN, Zhang ZQ, Qian XL (2001) Constraints on the supercontinental cycles: Evidence from Precambrian geology of North China Craton. Acta Petrol Sin 17:177–186 (in Chinese with English abstract)

Li XH, Li ZX, Ge WC, Zhou HW, Li WX, Liu Y, Wingate MRD (2003) Neoproterozoic granitoids in south China: Crustal

melting above a mantle plume at *ca*. 825 Ma? Precamb Res 122:45–83
Liu YS, Zhao CH (1991) The first discovery of fresh garnet lherzolite nodule from Pengjiabang kimberlite pipe in the Dahongshan area, Hubei Province. Geol Sci Technol Inf 10(Suppl):109–116 (in Chinese)
Liu GL, Wang XW, Lü XM (1993) Dahongshan lamproites. Geological Publishing House, Beijing, pp 186 (in Chinese with English abstract)
Liu YS, Gao S, Lee CT, Hu SH, Liu XM, Yuan HL (2005) Melt-peridotite interactions: Links between garnet pyroxenite and high-Mg# signature of continental crust. Earth Planet Sci Lett 234:39–57
Lu FX, Zheng JP, Chen MH (1998) Discussion on formation condition of diamonds. Earth Sci Front 5:125–131 (in Chinese with English abstract)
Ludwig KR (2003) ISOPLOT3.0: A geochronological toolkit for Microsoft Excel. Berkeley Geochronology Center Special Publication No. 4, pp 70
Lugmair GW, Marti K (1978) Lunar initial 143Nd/144Nd: differential evolution of the lunar crust and mantle. Earth Planet Sci Lett 39:349–357
Menzie MA, Xu YG (1998) Geodynamics of the North China Craton. In: Flower MFJ, Chung SL, Lo CH, Lee TY (eds) Mantle dynamics and plate interactions in east Asia. Am Geophys Union, Geodyn Series 100, pp 155–165
Menzies MA, Fan WM, Zhang M (1993) Paleozoic and Cenozoic lithoprobes and the loss of 120 km of Archean lithosphere, Sino-Korean craton, China. In: Prichard HM, Alabaster T, Harris NBW, Neary CR (eds) Magmatic processes and plate tectonics, vol 76. Geological Society, London, pp 71–81
McDonough WF (1990) Constraints on the composition of the continental lithospheric mantle. Earth Planet Sci Lett 101:1–18
McDonough WF, Sun SS (1995) Composition of the Earth. Chem Geol 120:223–253
Meisel T, Walker RJ, Irving AJ, Lorand JP (2001) Osmium isotopic compositions of mantle xenoliths: a global perspective. Geochim Cosmochim Acta 65:1311–1323
Mitchell RH, Keays RR (1981) Abundance of gold, palladium and iridium in some spinel and garnet lherzolites: implications for the nature of origin of precious metal-rich intergranular components in the upper mantle. Geochim Cosmochim Acta 45:2425–2442
O'Reilly SY, Griffin WL, Poudjom Djomani YH, Morgan P (2001) Are lithospheres forever? Tracking changes in sub-continental lithospheric mantle through time. GSA Today 11(4):4–10
Pearson DG (1999) The age of continental roots. Lithos 48:171–194
Pearson DG, Carlson RW, Shirey SB, Boyd FR, Nixon PH (1995) Stabilisation of Archaean lithospheric mantle: a Re–Os isotope study of peridotite xenoliths from the Kaapvaal craton. Earth Planet Sci Lett 134:341–357
Pollack HN (1986) Cratonization and thermal evolution of the mantle. Earth Planet Sci Lett 80:175–182
Qiu JS, Xu XS, Lo QH (2002) Potassium-rich volcanic rocks and lamprophyres in western Shandong Province: ^{40}Ar-^{39}Ar dating and source tracing. Chinese Sci Bull 47(2):91–99
Ravizza G, Pyle D (1997) PGE and Os isotopic analyses of single sample aliquots with NiS fire assay preconcentration. Chem Geol 141:251–268
Richardson SH, Gurney JJ, Erlank AJ, Harris JW (1984) Origin of diamonds in old enriched mantle. Nature 310:198–202
Richardson SH, Erlank AJ, Hart SR (1985) Kimberlite-borne garnet peridotite xenoliths from old enriched sub-continental lithosphere. Earth Planet Sci Lett 75:116–128
Rudnick RL, Fountain DM (1995) Nature and composition of the continental crust: a lower crustal perspective. Rev Geophys 33:267–309
Rudnick RL, Gao S, Ling WL, Liu YS, McDonough WF (2004) Petrology and geochemistry of spinel peridotite xenoliths from Hannuoba and Qixia, North China Craton. Lithos 77:609–637
Rudnick RL, Gao S, Yuan HL, Puchtel I, Walker R (2006) Persistence of Paleoproterozoic lithospheric mantle in the Central Zone of the North China Craton. Abstract for the International Conference on Continental Volcanism-IAVCEI, Guangzhou, China
Schoenberg R, Kramers JD (2000) Precise Os isotope ratio and Re–Os isotope dilution measurements down to the picogram level using multicollector inductively coupled plasma source mass spectrometry. Int J of Mass Spectrom 197:85–94
Shirey SB, Walker RJ (1998) The Re–Os isotope system in cosmochemistry and high-temperature geochemistry. Annu Rev Earth Planet Sci 26:423–500
Smith D, Boyd FR (1987) Compositional heterogeneities in a high-temperature lherzolite nodule and implications for mantle processes. In: Nixon PH (eds) Mantle Xenoliths. Wiley, Chichester, pp 551–561
Song Y, Frey FA (1989) Geochemistry of peridotite xenoliths in basalts from Hannuoba, Eastern China: implications for subcontinental mantle heterogeneity. Geochim Cosmochim Acta 53:97–113
Steiger RH, Jäger E (1977) Subcommission on geochronology; convention on the use of decay constants in geochronology and cosmochronology. Earth Planet Sci Lett 36:359–362
Sun M, Jain J, Zhou MF, Kerrich R (1993) A procedural modification for enhanced recovery of precious metals (Au, PGE) following nickel sulfide fire assay and tellurium co-precipitation: applications for analysis of geological samples by Inductively Coupled Plasma Mass Spectrometry. Can J Appl Spectrom 38:103–108
Tang YJ, Zhang HF, Ying JF (2004) High-Mg olivine xenocrysts entrained in Cenozoic basalts in central Taihang Mountains: relicts of old lithospheric mantle. Acta Petrol Sin 20(5):1243–1252 (in Chinese with English abstract)
Tompkins LA, Meyer SP, Han Z, Hu S, Armstrong R, Tayer WR (1999) Petrology and geochemistry of kimberlites from Shandong and Liaoning Provinces, China. In: Gurney JJ, Gurney JL, Pascoe MD, Richardson SH (eds) Proceedings of the 7th International Kimb Conf 2, pp 872–887
Walker RJ, Prichard HM, Ishiwatari A, Pimentel M (2002) The osmium isotopic composition of convective upper mantle deduced from ophiolite chromites. Geochim Cosmochim Acta 66:329–245
Wang JB (1991) Geochemistry of Daoxian basalts and its tectonic implication. Hunan Geol 11:52–58 (in Chinese)
Wang FZ, Li HL, Zhu QW, Lu FX (1997) Assemblages of anatectic xenoliths from volcanic and the petrology model of lithosphere in south Hunan province. Geol Sci Tech Inf 16:1–7 (in Chinese with English abstract)
Wang YJ, Fan WM, Zhang YH (2004) Geochemical, ^{40}Ar/^{39}Ar geochronological and Sr-Nd isotopic constraints on the origin of Paleoproterozoic mafic dikes from the southern Taihang Mountains and implications for the 1800 Ma event of the North China Craton. Precamb Res 135:55–79
Wang YJ, Fan WM, Peng TP, Zhang HF, Guo F (2005) Nature of the Mesozoic lithospheric mantle and tectonic decoupling beneath the Dabie Orogen, Central China: evidence from ^{40}Ar/^{39}Ar geochronology, elemental and Sr-Nd-Pb isotopic compositions of early Cretaceous mafic rocks. Chem Geol 220:165–189
Wilde SA, Zhou XH, Nemchin AA, Sun M (2003) Mesozoic crust-mantle interaction beneath the North China craton: a consequence of the dispersal of Gondwanaland and accretion of Asia. Geology 31:817–820
Wu FY, Walker RJ, Ren XW, Sun DY, Zhou XH (2003) Osmium isotopic constraints on the age of lithospheric mantle beneath northeastern China. Chem Geol 196:107–129

Wu FY, Lin JQ, Wilde SA, Zhang XO, Yang JH (2005) Nature and significance of the Early Cretaceous giant igneous event in eastern China. Earth Planet Sci Lett 233:103–119

Wu FY, Walker RJ, Yang YH, Yuan HL, Yang JH (2006) The chemical-temporal evolution of lithospheric mantle underlying the North China Craton. Geochim Cosmochim Acta 70:5013–5034

Xia QX, Zhi XC, Meng Q, Zheng L, Peng ZC (2004) The trace element and Re–Os isotopic geochemistry of mantle-derived peridotite xenoliths from Hannuoba: Nature and age of SCLM beneath the area. Acta Petrol Sin 20(5):1215–1224 (in Chinese with English abstract)

Xu YG (2001) Thermo-tectonic destruction of the Archean lithospheric keel beneath the Sino-Korean Craton in China: evidence, timing and mechanism. Phys Chem Earth (A) 26:747–757

Xu YG, Menzies MA, Vroon P, Mercier JC, Lin CY (1998) Texture-temperature- geochemistry relationship in the upper mantle as revealed from spine1 peridotite xenoliths from Wangqing, NE China. J Petrol 39:469–493

Xu YG, Ma JL, Huang XL, Iizuka Y, Chung SL, Wang YB, Wu XY (2004) Early Cretaceous gabbroic complex from Yinan, Shandong Province: petrogenesis and mantle domains beneath the North China Craton. Int J Earth Sci 93:1025–1041

Yan J, Chen JF, Xie Z, Zhou TX (2003) Mantle xenoliths from Late Cretaceous basalt in eastern Shandong Province: New constraint on the timing of lithospheric thinning in eastern China. Chin Sci Bull48(19):2139–2144

Ying JF, Zhou XH, Zhang HF (2004) Geochemical and isotopic investigation of the Laiwu-Zibo carbonatites from western Shandong Province, China and implications for their petrogenesis and enriched mantle source. Lithos 75:413–426

Ying JF, Zhang HF, Kita N, Morishita Y, Shimoda G (2006) Nature and evolution of Late Cretaceous lithospheric mantle beneath the eastern North China Craton: constraints from petrology and geochemistry of peridotitic xenoliths from Junan, Shandong province, China. Earth Planet Sci Lett 244:622–638

Yuan XC (1996) Atlas of geophysics in China. Geological Publishing House, Beijing, pp 217 (in Chinese)

Zhang HF (2005) Transformation of lithospheric mantle through peridotite-melt reaction: a case of Sino-Korean craton. Earth Planet Sci Lett 237:768–780

Zhang HF (2006) Complex peridotitic xenoliths: rare and important samples for understanding the lithospheric evolution. Earth Science 31(1):31–37 (in Chinese with English abstract)

Zhang HF, Sun M (2002) Geochemistry of Mesozoic basalts and mafic dikes in southeastern North China craton and tectonic implication. Int Geol Rev 44:370–382

Zhang HF, Yang YH (2007) Emplacement age and Sr-Nd-Hf isotopic characteristics of the diamondiferous kimberlites from the eastern North China Craton. Acta Petrol Sin 23(2):285–294 (in Chinese with English abstract)

Zhang AD, Xu DH, Xie XL, Guo LH, Zhou JX, Wang WY (1994) The status and future of diamond exploration in China. Proc Int Kimb Conf 2:264–269

Zhang HF, Sun M, Lu FX, Zhou XH, Zhou MF, Liu YS, Zhang GH (2001) Geochemical significance of a garnet lherzolite from the Dahongshan kimberlite, Yangtze Craton, southern China. Geochem J 35:315–331

Zhang HF, Sun M, Zhou XH, Fan WM, Zhai MG, Yin JF (2002) Mesozoic lithosphere destruction beneath the North China Craton: evidence from major, trace element, and Sr-Nd-Pb isotope studies of Fangcheng basalts. Contrib Mineral Petrol 144:241–253

Zhang HF, Sun M, Zhou XH, Zhou MF, Fan WM, Zheng JP (2003) Secular evolution of the lithosphere beneath the eastern North China Craton: evidence from Mesozoic basalts and high-Mg andesites. Geochim Cosmochim Acta 67:4373–4387

Zhang HF, Sun M, Zhou MF, Fan WM (2004) Highly heterogeneous Late Mesozoic lithospheric mantle beneath the North China Craton: evidence from Sr-Nd-Pb isotopic systematics of mafic igneous rocks. Geol Mag 141:55–62

Zhang HF, Sun M, Zhou XH, Ying JF (2005) Geochemical constraints on the origin of Mesozoic alkaline intrusive complexes from the North China Craton and tectonic implications. Lithos 81:297–317

Zhang HF, Ying JF, Tang YJ, Zhang J, Zhao XM, Niu LF, Xiao Y, Su BX (2006) Heterogeneity of Mesozoic and Cenozoic lithospheric mantle beneath the eastern North China Craton: evidence from olivine compositional mapping. Acta Petrol Sin 22(9):2279–2288 (in Chinese with English abstract)

Zhang HF, Ying JF, Shimoda G, Kita NT, Morishita Y, Shao JA, Tang YJ (2007) Importance of melt circulation and crust-mantle interaction in the lithospheric evolution beneath the North China Craton: evidence from Mesozoic basalt-borne clinopyroxene xenocrysts and pyroxenite xenoliths. Lithos 96:67–89

Zhao GC, Cawood PA, Wilde SA, Sun M (2000) Metamorphism of basement rocks in the Central Zone of the North China Craton: implications for Paleoproterozoic tectonic evolution. Precamb Res 103:55–88

Zhao GC, Wilde SA, Cawood PA, Sun M (2001) Archean blocks and their boundaries in the North China Craton: lithological, geochemical, structural and P-T path constraints and tectonic evolution. Precamb Res 107:45–73

Zhao GC, Sun M, Wilde SA, Li SZ (2005) Late Archean to Paleoproterozoic evolution of the North China Craton: key issues revisited. Precamb Res 136:177–202

Zheng JP, Lu FX (1999) Petrologic characteristics of kimberlite-borne mantle xenoliths from the Shandong and Liaoning Peninsula: Paleozoic lithosphere mantle and its heterogeneity. Acta Petrol Sin 15(1):65–74 (in Chinese with English abstract)

Zheng JP, O'Reilly SY, Griffin WL, Lu FX, Zhang M (1998) Nature and evolution of Cenozoic lithospheric mantle beneath Shandong peninsula, Sino-Korean craton, eastern China. Int Geol Rev 40:471–499

Zheng JP, O'Reilly SY, Griffin WL, Lu FX, Zhang M, Pearson NJ (2001) Relict refractory mantle beneath the eastern North China block: significance for lithosphere evolution. Lithos 57:43–66

Zheng JP, O'Reilly SY, Griffin WL, Zhang M, Lu FX, Liu GL (2004) Nature and evolution of Mesozoic-Cenozoic lithospheric mantle beneath the Cathaysia block, SE China. Lithos 74:41–65

Zheng JP, Griffin WL, O'Reilly SY, Zhang M, Pearson N (2006a) Zircons in mantle xenoliths record the Triassic Yangtze—North China continental collision. Earth Planet Sci Lett 247:130–142

Zheng JP, Griffin WL, O'Reilly SY (2006b) Mineral chemistry of garnet peridotites from Paleozoic, Mesozoic and Cenozoic lithosphere: constraints on mantle evolution beneath Eastern China. J Petrol 47:2233–2256

Zheng JP, Griffin WL, O'Reilly SY, Zhang M, Pearson N, Pan YM (2006c) Widespread Archean basement beneath the Yangtze craton. Geology 34:417–420

Zheng JP, Griffin WL, O'Reilly SY, Yang JS, Zhang RY (2006d) A refractory mantle protolith in younger continental crust, east-central China: Age and composition of zircon in the Sulu UHP peridotite. Geology 34:705–708

Zheng YF, Zhao ZF, Wu YB, Zhang SB, Liu XM, Wu FY (2006e) Zircon U-Pb age, Hf and O isotope constraints on protolith origin of ultrahigh-pressure eclogite and gneiss in the Dabie orogen. Chem Geol 231:135–158

Zhi XC, Qin X (2004) Re–Os isotope geochemistry of the mantle-derived peridotite xenoliths from eastern China: constrains on

the age and thinning of lithospheric mantle. Acta Petrol Sin 20:989–998 (in Chinese with English abstract)

Zhi XC, Peng ZC, Chen DG, Yu CJ, Sun WD, Reisberg L (2001) The longevity of subcontinental lithospheric mantle beneath Jiangsu-Anhui region. Sci in China (D) 44:1110–1118

Zhou MF (1994) PGE distribution in 2.7 Ga layered komatiite flows from the Belingwe greenstone belt, Zimbabwe. Chem Geol 118:155–172

Zhou MF, Yumul GP, Malpas J, Sun M (2000) A comparative study of platinum-group elements in the Coto and Acoje Blocks of the Zambales Ophiolite Complex, Philippines. Isl Arc 9:557–565

Zhou MF, Yan DP, Kennedy AK, Li YQ, Ding J (2002) SHRIMP U-Pb zircon geochronological and geochemical evidence for Neoproterozoic arc-magmatism along the western margin of the Yangtze Block, South China. Earth Planet Sci Lett 196:51–67